

**Magnitude and Location of Historical Earthquakes in Japan and Implications
for the 1855 Ansei Edo Earthquake**

William H. Bakun
U.S. Geological Survey
345 Middlefield Road MS977
Menlo Park CA 94025

Abstract

Japan Meteorological Agency (*JMA*) intensity assignments I_{JMA} are used to derive intensity attenuation models suitable for estimating the location and an intensity magnitude M_{jma} for historical earthquakes in Japan. The intensity for shallow crustal earthquakes on Honshu is equal to $-1.89 + 1.42M_{JMA} - 0.00887\Delta_h - 1.66\log\Delta_h$, where M_{JMA} is the JMA magnitude, $\Delta_h = (\Delta^2 + h^2)^{1/2}$, and Δ and h are epicentral distance and focal depth (km), respectively. Four earthquakes located near the Japan Trench were used to develop a subducting-plate intensity attenuation model where intensity is equal to $-8.33 + 2.19M_{JMA} - 0.00550\Delta_h - 1.14\log\Delta_h$. The I_{JMA} assignments for the M_{JMA} 7.9 Great 1923 Kanto earthquake on the Philippine Sea-Eurasian plate interface are consistent with the subducting-plate model; Using the subducting-plate model and 226 I_{JMA} IV-VI assignments, the location of the intensity center is 25 km north of the epicenter, M_{jma} is 7.7, and M_{JMA} is 7.3 to 8.0 at the 1σ confidence level. Intensity assignments and reported aftershock activity for the enigmatic 11 November 1855 Ansei Edo earthquake are consistent with an M_{JMA} 7.2 Philippine Sea-Eurasian interplate source or Philippine Sea intraslab source at about 30 km depth. If the 1855 earthquake was a Philippine Sea-Eurasian interplate event, the intensity center was adjacent to and downdip of the rupture area of the Great 1923 Kanto earthquake, suggesting that the 1855 and 1923 events ruptured adjoining sections of the Philippine Sea-Eurasian plate interface.

Introduction

The twelve million residents of metropolitan Tokyo feel earthquakes almost every week. Most of these felt earthquakes are small and cause little damage, but some (*e.g.*, the Great 1923 Kanto and 1855 Ansei Edo earthquakes) have devastated Tokyo. Tokyo is built atop the triple junction of the Eurasian plate, the Philippine Sea (PHS) plate, and the Pacific (PAC) plate (Fig. 1a). The PHS plate is subducting beneath the Eurasian plate and the PAC plate is subducting beneath the PHS and Eurasian plates (*e.g.*, Ishida, 1992). [Plate boundaries on Honshu are controversial. Noguchi (2002), for example, describes the convergence of four plates and two triple junctions.] Earthquakes felt in Tokyo occur as shallow crustal events, as PHS- Eurasian interplate events, as PAC-PHS/Eurasian interplate events, as PHS intraplate events, and as PAC intraplate events. Even earthquakes associated with eruptions of nearby volcanoes are felt in Tokyo.

Seismicity near Tokyo has been monitored by seismographs for about 100 years. Focal depths and mechanisms are available for many earthquakes during this period, so that the provenance of recent significant earthquakes can be incorporated into the tectonic models with which seismic hazard is estimated. That is, we know, or think we know, the major source zones of future earthquakes that might cause serious damage in Tokyo. We do not know, however, how often large earthquakes occur on each seismogenic structure, whether the interevent times are regular, and, in some cases, the time and magnitude of the last significant earthquake. Some of this critical hazard information might be gathered from excavations of shallow onshore faults, from uplifted marine terraces (*e.g.*, Matsuda *et al.*, 1978) and from preserved tsunami deposits (Fujiwara *et al.*, 2000). The main source of seismic hazard information, however, is the accounts of the effects of historical earthquakes –accounts that potentially extend the instrumental record of earthquakes near Tokyo back an additional 500+ years.

Damage and other effects of earthquakes in Japan are codified by Japan Meteorological Agency (*JMA*) in an intensity scale. *JMA* magnitudes and *JMA* intensities are represented herein by M_{JMA} and I_{JMA} , respectively. The I_{JMA} scale, used only in Japan, is different from the

Modified Mercalli (MM) intensity scale (Wood and Neumann, 1931) used in the USA and many other countries and the MSK (Medvedev *et al.*, 1967) and ESC intensity scales (Grünthal, 1998) prevalent in most of Europe. The most important difference is that I_{JMA} effectively ranges from I (felt under favorable circumstances) to VI (severe damage to ordinary well-built buildings), while the MM, MSK, and ESC scales range from I to IX for similar effects (Musson, 1999). (The maximum level on the I_{JMA} scale was extended from VI to VII after the 1948 Fukui earthquake, and intensity VII was first used to describe the effects of the 1995 Kobe earthquake.) Thus, I_{JMA} is a coarser binning of earthquake effects, resulting in lower resolution of earthquake parameters estimated from intensity assignments than elsewhere. For example, hundreds of MSK assignments are often listed for even small earthquakes in France. MSK intensities are routinely assigned at half unit intervals and rated using a four-factor quality scale and reliable, high-resolution estimates of the location and magnitude of historical earthquakes in France are generally available (Bakun and Scotti, in preparation). Although such intensity data sets do not exist for earthquakes in Japan, objective estimates of the location and magnitude of historical earthquakes are still possible.

Many authors have analyzed and interpreted the accounts of historical earthquakes in Japan. Current efforts to systematically extract a consistent, complete catalog of earthquakes from the historical accounts incorporate results of Professor Tokuji Utsu's extensive studies of intensities of Japanese earthquakes. Utsu (1984) obtained an empirical relation between I_{JMA} and epicentral distance Δ and M_{JMA} for shallow onshore earthquakes. He then developed similar relations for upper mantle earthquakes with focal depths h between 40 and 80 km, excluding those off the Pacific coast of eastern Japan (Utsu, 1986), and for earthquakes off the Pacific coast of eastern Japan with focal depths h between 0 and 80 km (Utsu, 1987). The rate of decay of I_{JMA} with Δ is less in Utsu's (1987) model for PAC plate events than for his other models (Utsu, 1984; 1986). Utsu (1984; 1986; 1987) assumed for a given M_{JMA} that I_{JMA} decreases linearly with Δ , a functional form that accounts for attenuation and scattering of seismic energy with increasing Δ , but not for geometrical spreading. Geometrical spreading is important in modeling intensities at Δ less than 100 km. Utsu (1988) then investigated the relation between epicentral intensity and h and M_{JMA} and proposed empirical relations for estimating M_{JMA} given the epicentral intensity and h .

Bakun and Wentworth (1997) developed techniques for estimating the location and M_w of historical earthquakes in California with MM intensity assignments. Bakun and Wentworth's (1997) techniques have been applied successfully in other regions of the USA (*e.g.*, Bakun, 2000; Bakun *et al.*, 2002; Bakun and Hopper, 2004a;b) and in Turkey (Parsons *et al.*, 2000), Germany (Hinzen and Oemisch, 2001), Switzerland (Swiss Seismological Service, 2002), and France (Bakun and Scotti, in preparation). Here I adapt these techniques to the I_{JMA} scale and to the estimation of location and magnitude of historical earthquakes in Japan. I start with the shallow earthquakes on Honshu (Eurasian plate events) and proceed to PAC and PHS interplate and intraplate events. Finally, I analyze the intensity data for the Great 1923 Kanto and the 1855 Ansei Edo earthquakes that devastated Tokyo. The analysis of additional historical earthquakes near Tokyo and the development of a catalog of historical earthquakes are the topics of future work.

Calibration Events

I_{JMA} for fourteen shallow events within about 300 km of Tokyo (Table 1 and Fig. 1) are used to calculate the attenuation of seismic energy with Δ . The intensity assignments are adequately sampled for $M_{JMA} < 7.0$ earthquakes at $\Delta < 400$ km (Fig. 2). Note that the intensities for an $M_{JMA} 7.3$ test event are consistent with the attenuation relation obtained for the calibration event intensities (see Fig. 5).

M_{jma} represents intensity magnitudes that are the best estimate of M_{JMA} using intensity assignments. The M_{JMA} and the JMA epicenters are standards against which the M_{jma} and the locations estimated from intensity assignments are judged. The average difference between M_{JMA} and moment magnitude M_w (Kanamori, 1977; Hanks and Kanamori, 1979) is insignificant for shallow M5-7 earthquakes and the standard deviation of $(M_{JMA} - M_w)$ is about ± 0.2 (Katsumata, 1996). Based on a comparison of scalar moments (Ekström, 1987; Sipkin, 1987),

the standard deviation of M_w is ± 0.08 so that the standard deviation of M_{JMA} is about ± 0.2 . Differences between M_{jma} and M_{JMA} less than about 0.2 are not significant.

Errors in JMA epicenters for shallow inland M6 earthquakes after the early 1930's probably do not exceed 5 km (N, Hamada, written comm., 2004). The source dimension of M6 and larger events is, however, greater than 5 km so that the moment centroid, the best point location of the source of strong shaking, may be more than 5 km from the epicenter. The moment centroid, however, is only available for some recent events. Although the JMA epicenters are the best available location standard, even a source location tens of kilometers distant from the JMA epicenter may not signify a mistaken location for a large earthquake.

Attenuation of Seismic Intensity

Intensity increases with the amplitude and duration of ground shaking, and depends on the period of the causative shaking, but there is no generally accepted relation of intensity to any specific ground-motion parameter. Intensity tends to increase with earthquake magnitude and decrease with Δ . The variation in intensity assignments at the same Δ can be attributed to azimuthal variations in the radiated energy, differences in wave propagation through crustal and upper-mantle structure, and near-site amplification factors, including the geologic foundation beneath the site and the sensitivity of the built environment and observers. That is,

$$\text{Intensity} = f(M) + g(\Delta) + k(\text{site}), \quad (1)$$

where $f(M)$, $g(\Delta)$, and $k(\text{site})$ represent the dependence of intensity on magnitude M , Δ , and site-specific characteristics, respectively. I estimate $f(M)$ and $g(\Delta)$, explicitly seeking to minimize site effects; site effects will be estimated and incorporated later as site corrections. Median Δ are used to characterize the intensity data because site effects are minimized in the median Δ (Bakun and Wentworth, 1997). Median Δ for each intensity level for each calibration event for which there were at least seven I_{JMA} assignments are used, and source depth h is accounted for by

calculating a slant distance $\Delta_h = (\Delta^2 + h^2)^{1/2}$. A more relevant depth is that of the moment centroid, which is available for some recent events, but generally not for historical earthquakes. For consistency, $h = 5$ km is assumed for all shallow events. The resulting median Δ_h are listed in Table 1.

Attenuation Model

$$\text{Let } g(\Delta_h) = C_1\Delta_h + C_2\log\Delta_h. \quad (2)$$

C_1 can be associated with intrinsic attenuation and scattering, and C_2 with geometric spreading. I used Joyner and Boore's (1993) one-stage maximum likelihood method developed for regression analysis of strong-motion data to fit the 36 median Δ_h to obtain the *Honshu* model:

$$I_{\text{PRED}} = -(1.89 \pm 2.44) + (1.42 \pm 0.12)M_{\text{JMA}} - (0.00887 \pm 0.00322)\Delta_h - (1.66 \pm 1.23)\log\Delta_h, \text{ where } \Delta_h \text{ is in km.} \quad (3)$$

Both intrinsic attenuation and geometric spreading contribute to the decrease of intensity with distance, but there is considerable tradeoff between coefficients C_1 and C_2 in the regression analysis. The coefficients in (3) cannot easily be related to intensity attenuation relations for other regions because the I_{JMA} scale differs from intensity scales used elsewhere (Musson, 1999). There are no clear systematic biases in the predicted intensities with magnitude, location, date, distance, or intensity level (Fig. 3). The attenuation model is consistent with the I_{JMA} assignments and median Δ_h for the calibration events (Fig. 4), and for the four independent shallow test events (Table 2 and Fig. 5).

Site Corrections

Following Bakun and Wentworth (1997), I assume that site effects can be represented as a constant additive correction to the I_{JMA} assignments, and that the correction does not change with date, epicenter location or event magnitude. That is, one correction is applicable for all I_{JMA} assigned at a particular site, but the correction may be significantly different at nearby sites. A

site correction for site i , $\delta I_{JMA(i,j)}$, is the mean $\{ I_{JMA(i,j)} - I_{pred,i} \}$ for j calibration events, where $I_{JMA(i,j)}$ is the I_{JMA} assignment at site i for event j , and $I_{pred,i}$ is the value of I_{JMA} calculated using (3) with the M_{JMA} and the epicenter locations in Table 1. $\delta I_{JMA(i,j)}$ were calculated for 73 sites where I_{JMA} assignments for more than one calibration event are available. The site corrections are relatively well determined because intensity assignments for several calibration events are available at many sites; intensity assignments for all 14 calibration events are available only at JMA site *Kofu Iida*, a suburb of Kofu. MM intensity site corrections in the southern San Francisco Bay region, California, are weakly correlated with soil stiffness, with negative corrections (less than predicted intensity) for sites underlain by the stiffest material (shear-wave velocity $\beta > 700\text{m/sec}$) and positive corrections (greater than predicted intensity) for sites underlain by very soft soils ($\beta = 100\text{-}200\text{m/sec}$) (Bakun and Wentworth, 1997).

Estimating Location and Magnitude

I will analyze the I_{JMA} assignments using the technique of Bakun and Wentworth (1997). First, calculate the intensity magnitude M_{jma} and rms $[M_{jma}]$ over a grid of trial epicenter locations.

$$M_{jma} = \text{mean} (M_i), \quad (4)$$

where

$$M_i = \{ I_{JMA,i} - \delta I_i + 1.89 + 0.00887(\Delta_h)_i + 1.66 \log(\Delta_h)_i \} / 1.42 \quad (5)$$

and $I_{JMA,i}$, δI_i , and $(\Delta_h)_i$ are the I_{JMA} assignment, empirical I_{JMA} site correction, and focal distance (km) at site i , respectively. δI_i is 0 if δI_i is not available.

$$\text{rms} [M_{jma}] = [\text{rms} (M_{jma} - M_i) - \text{rms}_0(M_{jma} - M_i)], \quad (6)$$

where $\text{rms} (M_{jma} - M_i) = \{\sum_i [W_i(M_{jma} - M_i)]^2 / \sum_i W_i^2\}^{1/2}$, $\text{rms}_0 (M_{jma} - M_i)$ is the minimum rms ($M_{jma} - M_i$) over the grid of trial epicenters, and W_i is Bakun and Wentworth's (1997) distance weighting function:

$$W_i = \begin{cases} 0.1 + \cos [(\Delta_i/150)(\pi/2)] & \text{for } \Delta_i < 150 \text{ km} \\ 0.1 & \text{for } \Delta_i \geq 150 \text{ km.} \end{cases} \quad (7)$$

The intensity center is the trial source location for which rms [M_{jma}] is minimum (Bakun, 1999). The intensity center corresponds more to the moment centroid than to the epicenter.

The rms [M_{jma}] contours provide a basis for identifying regions of likely epicenter location. For earthquakes with sufficient intensity assignments, the rms [M_{jma}] contours bound the epicentral region. Bakun and Wentworth (1997) associated rms contour values for earthquakes in California with confidence levels that the epicenter was within the contour, as tabulated in the corrected Table 5b of Bakun and Wentworth (1999). M_{jma} at trial locations within the appropriate confidence-level contours are the best estimates of M_{JMA} for these source locations.

Estimates of Magnitude and Location –Calibration Events

M_{jma} for the calibration events, calculated using (4) and the epicenter locations in Table 1, are listed in Table 3. Ignoring site corrections, the mean ($M_{JMA} - M_{jma}$) is -0.04 and the standard deviation of ($M_{JMA} - M_{jma}$) is 0.17 . If site corrections are included, the mean and standard deviation are -0.03 and 0.16 , respectively. Without site corrections, the mean distance between intensity centers and epicenters is 47.3 km. With site corrections, the mean distance is 35.1 km. The distances of the intensity centers from the epicenters are smaller for 13 of the 14 calibration events when site corrections are used. M_{jma} at the intensity centers are also listed in Table 3. With site corrections, the mean ($M_{JMA} - M_{jma}$) is -0.02 and the standard deviation of ($M_{JMA} - M_{jma}$) is 0.21 . The I_{JMA} site corrections are not available for historical earthquakes because

intensities are not assigned at JMA sites for earthquakes before 1926. Without site corrections, the mean ($M_{JMA} - M_{jma}$) is -0.10 and the standard deviation of ($M_{JMA} - M_{jma}$) is 0.25 . M_{jma} at the intensity center of historical earthquakes provide estimates of M_{JMA} with an uncertainty of 0.25 .

Estimates of Magnitude and Location –Test Events

The intensity assignments and the median Δ_n for the four test events (Table 2) are consistent with (3), the Honshu intensity attenuation model (Fig. 5). There is little difference in the M_{jma} estimated for the test events for locations at the hypocenter, for locations at the intensity center without site corrections, and for locations at the intensity center with site corrections (Table 2). The agreement of M_{jma} and M_{JMA} for the four test events is better than for the calibration events (Tables 2 and 3; Fig. 6).

Although the distance of the epicenters of the test events from the intensity centers calculated using site corrections range from 10 to 80 km (Table 2), the epicenters are within the 95% confidence contour for location appropriate for a comparable number of intensity assignments for earthquakes in California (Fig. 7). The confidence contours for location appropriate for California earthquakes with MM intensity assignments are not appropriate, however, for earthquakes in Japan with I_{JMA} assignments.

The location uncertainties for earthquakes in Japan can be estimated using a bootstrap-resampling test (Efron, 1982), with 1,000 resampling calculations of the intensity center, each using N random samples of the I_{JMA} data set with replacement, where N is the number of I_{JMA} assignments. The bootstrap intensity centers for the test events, with and without site corrections, are shown in Figure 8. The red rms[M_{jma}] contours enclose 67% of the bootstrap resampling intensity centers, and can be interpreted as the 1σ location error contours. In fact, six of the epicenters in the eight cases shown in Figure 8 are within the 67% contours. The spatial distribution of bootstrap intensity centers for earthquakes in the United States mimics the rms contours (Bakun *et al.*, 2002; Bakun and Hopper, 2004a), and the fraction of bootstrap intensity centers within the confidence contours are consistent with the confidence levels suggested by

Bakun and Wentworth (1999). Surprisingly, there is no comparable correspondence between the distributions of bootstrap intensity centers and rms $[M_{jma}]$ contours in Figure 8. Furthermore, application of site corrections does not concentrate the bootstrap intensity centers closer to the intensity center, as might be expected. However, epicenters for all four events lie within the 1σ error contour if site corrections are used, and only two of the four epicenters lie within the 1σ error contour when site corrections are not used.

The M_{jma} for those bootstrap intensity centers within the 1σ contours can be used to estimate the uncertainty in M_{jma} (Fig. 9). The standard deviations of M_{jma} with site corrections range from 0.09 for events #T1 and T4 to 0.17 for event #T3. The uncertainty in M_{jma} is interesting, but the uncertainty in M_{JMA} estimated from intensity observations is more important. The uncertainty in M_{JMA} can be estimated from the standard deviation of M_{jma} and the standard deviation $(M_{JMA} - M_{jma}) = 0.16$ for the calibration events evaluated at the epicenter. Since these errors are independent, $\sigma^2(M_{JMA})$, where M_{JMA} is estimated from the I_{JMA} assignments, is $\sigma^2(M_{jma}) + 0.16^2$. That is, $\sigma(M_{JMA}) = 0.18, 0.21, 0.23,$ and 0.18 for events #T1, T2, T3, and T4, respectively. These uncertainties are consistent with the standard deviation of $(M_{JMA} - M_{jma})$ listed for the calibration events in Table 3. Similar standard deviations of M_{jma} are obtained without site corrections (0.09 for #T1; 0.13 for #T2; 0.17 for #T3; and 0.09 for #T4). Using the standard deviation $(M_{JMA} - M_{jma}) = 0.17$ for the calibration events evaluated at the epicenter without site corrections, $\sigma(M_{JMA}) = 0.20, 0.20, 0.23,$ and 0.19 for events #T1, T2, T3, and T4, respectively. These uncertainties are all marginally smaller than the standard deviation of $(M_{JMA} - M_{jma}) = 0.25$, where M_{jma} is evaluated at the intensity center without site corrections. M_{JMA} can be estimated from I_{JMA} assignments with a 1σ uncertainty of 0.2-0.3.

Additional Shallow Test Earthquakes

Thirty-two additional shallow test events (Table 4) were selected to test the techniques described above in other regions of Japan (events #T5-T26) and instrumental I_{JMA} assigned for earthquakes after April 1996 (events #T27-T36).

Magnitude estimates. ($M_{JMA} - M_{jma}$) for M_{jma} calculated for sources at the epicenters show a consistent spatial pattern (Fig. 1b). M_{jma} is an unbiased estimate of M_{JMA} for events in central Honshu, and for events on and near Shikoku and Kyushu Islands in southwest Japan. M_{JMA} is greater than M_{jma} for the 23 January 1975 event (#T22) in central Kyushu and for the 3 September 1998 event (#T30) in northern Japan. The 23 January 1975 event was the largest in an earthquake swarm on the northern rim of Mt. Aso caldera (Kubotera and Mitsunami, 1980). Aso caldera is one of the largest in the world and contains more than 17 volcanoes (Kubotera and Mitsunami, 1980). Low P and S velocities are associated with magma chambers beneath Mt. Aso caldera (Sudo and Kong, 2001). The epicenter of the 3 September 1998 earthquake is about 10 km southwest of Iwate Volcano, and the earthquake was triggered by inflation of the volcano (Nishimura *et al.*, 2001).

In contrast, M_{jma} is greater than M_{JMA} in other regions, such as in southwest Honshu near the coast of the Sea of Japan (Fig. 1b). The cause of the $M_{JMA} - M_{jma}$ mismatch does not appear to be a significantly different rate of change of I_{JMA} with Δ (Fig. 10). Rather, the Honshu model is offset vertically from the I_{JMA} data. For example, the I_{JMA} are about 0.6 I_{JMA} units too large for the 1943 Tottori earthquake (#T9 in Fig. 10). It is unlikely that the I_{JMA} or the M_{JMA} scales differ significantly across Japan, so perhaps earthquakes in these other regions generate relatively more high-frequency energy that is reflected in greater I_{JMA} assignments. Atkinson and Hanks (1995) suggested that more high-frequency energy might be explained by higher stress drop sources. Kanamori and Allen (1986) noted that earthquakes with longer repeat times, like the 1943 Tottori earthquake, tend to have shorter fault lengths, and consequently higher stress drops. M_{jma} is consistently greater than M_{JMA} for the 1943 Tottori event and the other events occurring in southwest Honshu near the coast of the Sea of Japan (Fig. 1b). This region is characterized by faults with very low slip rates or undefined slip rates (Research Group for Active Faults in Japan, 1991) so higher stress drops and M_{jma} greater than M_{JMA} for earthquakes in this region of Japan should not be surprising.

Location estimates. Locations estimated from the $\text{rms}[M_{\text{jma}}]$ for the test events in other regions (Fig. 11) are comparable to those for test events near Tokyo (Fig. 8, left column). There is little control in the location of events outside the network of intensity sites (Bakun, 2000), even though the intensity center for the Sea of Japan event (#T25) is near the epicenter. The epicentral region for event #T22 is surrounded by I_{JMA} sites and the epicenter is 13 km from the intensity center. On the other hand, the epicenter for event #T9 is 72 km north of its intensity center, comparable to the 83 km epicenter-to-intensity center distance obtained for event #T3 (compare Figs. 11a and 8c, left).

Shallow Test Earthquakes, 1997-2000. In April 1996, JMA changed its procedures for assigning intensities from accounts of the effects of earthquakes on people, buildings, and the earth surface to an interpretation of recorded ground motions. $(M_{\text{JMA}} - M_{\text{jma}})$ for the three Izu events are consistent with $(M_{\text{JMA}} - M_{\text{jma}})$ for the calibration events in the same area. $(M_{\text{JMA}} - M_{\text{jma}}) = -0.2$ for the 1997 $M_{\text{JMA}} 6.6$ (#T28) and 2000 $M_{\text{JMA}} 7.3$ (#T36) events located near the coast of the Sea of Japan; the data for these events are consistent with other events in this region (Fig. 1b). $(M_{\text{JMA}} - M_{\text{jma}})$ is 0.3 for the 1997 $M_{\text{JMA}} 5.7$ Izu events (#T27 and #T29). M_{jma} is in general agreement with M_{JMA} for 1997-2000 events, suggesting that the traditional and post-April 1996 instrument-based I_{JMA} assignments are generally consistent.

Five phreatic eruptions of Miyakejima and a swarm of thousands of earthquakes beneath the Izu volcanic islands occurred in 2000 (Toda *et al.*, 2002). Intensity data for the five $M_{\text{JMA}} > 6.0$ earthquakes in the swarm are shown in Figure 12. Three of these events (Fig. 12a) occurred near the location of Toda *et al.*'s (2002) modeled magmatic dyke, while the other two events occurred to the north and to the south of the dyke. $(M_{\text{JMA}} - M_{\text{jma}})$ is 0.6, 0.3, and, 0.4 for the 3 events located near the dyke, 0.0 for the event north of the dyke, and -0.1 for the event south of the dyke (Fig. 1b, *inset*). That is, the I_{JMA} are less than expected for the three events located near the magmatic dyke and as expected for the two events located 10 km or so off the dyke. The positive $(M_{\text{JMA}} - M_{\text{jma}})$ for the three near-dyke events, for the 23 January 1975 event (#T22) near Mt. Aso, and for the 3 September 1998 event (#T30) near Iwate Caldera are comparable and might be explained by anomalous near-source attenuation of shear-waves propagating through

highly-attenuating hot, cracked magmatic rock or by near-volcano sources which generate less high frequency energy than other earthquakes on Honshu.

Subducting-plate model. There is significantly stronger shaking for subducting-plate earthquakes than for shallow crustal events (compare Fig. 13 and Figs. 4, 5, and 10). Nakamura *et al.*'s (1994) 3-D attenuation structure of Japan features high-velocity, high-Q PAC and PHS plates. The decay of I_{JMA} with Δ for PAC plate events is estimated using median Δ_h for four test events near the Japan Trench (#T6, T12, T19, and T20). As with the development of the Honshu model, median Δ_h were used for intensity levels with at least seven I_{JMA} assignments. The offshore locations of the events restrict the distance range of available I_{JMA} assignments so that some median Δ_h are potentially biased. Following Bakun *et al.* (2002), five median Δ_h with seven or more assignments (#T6: I_{JMA} =I and IV; #T12: I_{JMA} =III; #T19: I_{JMA} =I and V; #T20: I_{JMA} =I) were not used in the regression analysis. The remaining nine median Δ_h were then fit using Joyner and Boore's (1993) one-stage maximum likelihood method to obtain the *subducting-plate* model:

$$I_{\text{PRED}} = -(8.33 \pm 14.47) + (2.19 \pm 0.32)M_{JMA} - (0.00550 \pm 0.00684)\Delta_h - (1.14 \pm 6.65)\log\Delta_h, \text{ where } \Delta_h \text{ is in km.} \quad (8)$$

There is considerable tradeoff in the parameters of the subducting-plate model, but the median Δ_h and the I_{JMA} assignments for the four events near the Japan Trench are consistent with the subducting-plate model (Fig. 13a-13d and Table 4). The subducting-plate model is dramatically different from the Honshu model, and it is clear that significantly different M_{jma} will be obtained with the two models. For example, $(M_{JMA} - M_{jma})$ is -1.2 , -0.7 , -1.6 , and -1.2 for events #T6, T9, T19, and T20, respectively, if the Honshu model were used, rather than -0.2 , 0.0 , 0.1 , and 0.1 .

I_{JMA} for the 21 Sept 1968 $M_{JMA}6.9$ (#T37) and for the 17 Dec 1987 $M_{JMA}6.7$ (#T38) events are consistent with the subducting-plate model (Fig. 13e and 13f). The 21 Sept 1968 event occurred at 80 km depth, and earthquakes deeper than 50 km predominantly represent failure within descending slabs (Kirby *et al.*, 1996). That is, the 21 September 1968 event was a PAC-plate intraslab source. The 17 Dec 1987 event was an intraslab earthquake that occurred at 47 km depth within the PHS plate (Okada and Kasahara, 1990). The subducting-plate model is applicable to intermediate-depth intraslab events in both the PAC and PHS plates. The intensity center for the 1987 event is located 24 km southwest of the epicenter. Intensity centers obtained

using the subducting-plate model apparently provide useful estimates of the source locations of intraslab events occurring near Tokyo.

The Great 1923 Kanto earthquake. The hypocenter (35.328°N, 139.139°E, 23 km depth) of the 1 September 1923 $M_{JMA}7.9$ Kanto earthquake (JMA, 2004) lies near the northwest edge of a northeast-dipping fault plane that has been associated with the PHS-Eurasian plate interface (*e.g.*, Kanamori, 1971; Ando, 1971, 1974; Matsu'ura *et al.*, 1980); Wald and Somerville, 1995). The PHS-Eurasian plate interface has been relatively aseismic in recent decades so there is insufficient data to derive an intensity attenuation model using PHS plate events. One might expect that the primary characteristics of the subducting-plate model are applicable to PHS-Eurasian interplate events. That is, because the subducting PAC and PHS plates both serve as high-velocity low-attenuation waveguides (Nakamura *et al.*, 1994), I_{JMA} for sites on Honshu may be amplified in comparable fashion for earthquakes on the subducting PAC and PHS plates.

The JMA intensity database contains 44 intensities assigned at meteorological stations. I used these and 479 intensities assigned at auxiliary meteorological stations from an original hand-written JMA document (N. Hamada, written comm., 2004). The I_{JMA} for the 1923 Kanto earthquake relative to the Honshu and subducting-plate models for an $M_{JMA} 7.7$ source are shown in Figure 14. The I_{JMA} assignments are consistent with the subducting-plate model and inconsistent with the Honshu model. The remarkable difference between the models for crustal earthquakes and subducting-plate events explains why interplate events, like the Great 1923 Kanto earthquake, and intermediate-depth intraslab events in Japan can be particularly devastating if located near populated areas.

There are few assignments at $\Delta_h > 500$ km so the median Δ_h shown for I_{JMA} I, II, and III in Figure 14 are lower-bound estimates and M_{jma} calculated using these data will be lower-bound estimates of M_{JMA} . For historical earthquakes where the collection of intensity data is incomplete, the best estimate of intensity magnitude is obtained using those subsets of intensity assignments that are complete (Bakun and Scotti, in review). The I_{JMA} I, II, and III levels are not

sufficiently sampled at $\Delta > 500$ km so only the 226 I_{JMA} IV, V, and VI assignments are used to estimate source parameters for the Great 1923 Kanto event (Fig. 15). The intensity center (35.55°N, 139.18°E) is 25 km north of the epicenter and within the source rupture zone as modeled by Kanamori (1971), Ando (1971, 1974), Matsu'ura *et al.* (1980), Wald and Somerville (1995), Nyst *et al.* (2004), and Pollitz *et al.* (2004). The epicenter is near the south edge of the 67% confidence region for location (Fig. 16). M_{jma} is 7.7 at the epicenter and at the intensity center. Using the $1\sigma = 0.25$ uncertainty in M_{JMA} estimated from I_{JMA} assignments without site corrections, M_{JMA} is 7.3 to 8.0 at the 1σ confidence level.

1855 Ansei Edo earthquake. As an example historical earthquake, consider the enigmatic, highly-destructive 11November 11 1855 Ansei Edo earthquake. It is clear from the pattern of damage reports that the source is near Tokyo (*e.g.*, Usami, 1996), but the focal depth and causative seismogenic structure are controversial. Hagiwara (1972) inferred a depth of about 30 km from the pattern of intensity observations in Tokyo. Ohtake (1980) and Kasahara (1985) suggested that the 1855 Ansei Edo event occurred on the PHS-Eurasian interface on the down-dip extension of the rupture surface of the Great1923 Kanto earthquake. Hikita and Kudo (2001) simulated the intensity pattern in Tokyo using an empirical Green's function method and inferred a location near the top of the PAC plate. Recently Nakamura *et al.* (2003) concluded that the event was an intraslab PHS plate event. Furumura (2003) has suggested that intensities in Tokyo are largely controlled by effects of the thick sedimentary basin and are insensitive to source depth and that depth, and causative seismogenic structure, might be better inferred from intensities over a broader region.

Furumura (2003) simulated wave propagation within a 3-D structural model of the crust and upper plate near Tokyo for sources at 8 km, 35 km, and 70 km depth. He found that crustal events generate large amplitude Lg waves propagating in the crust over distances of about 150 km and that intermediate-depth events generate weak Lg waves. Deeper events generate large impulsive S waves that are efficiently propagated in the high-Q subduction plate to distant sites north of Tokyo (Furumura, 2003), which is consistent with the subducting-plate model.

Furumura (2003) used his simulations to conclude that the pattern of isoseismals for the 1855 Ansei Edo event is typical of shallow crustal earthquakes in Japan.

Intensity centers for three depth models calculated using Usami's (1996) intensity assignments for the 1855 Ansei Edo earthquake are only a few kilometers apart, but the M_{jma} range from 7.2 to 7.7 (Fig. 17). The model for a PHS-Eurasian interplate source (Fig. 18a), and a shallow crustal source (Fig. 18c) both apparently fit the intensity IV-VI assignments. The model for a PHS-Eurasian interplate source at 30 km depth (Fig. 18a) and for a PAC-plate source at 70 km depth (Fig. 18b) fit the intensity III assignments, but the model for a shallow crustal event does not (Fig. 18c). In particular, the intensity III assignments extend farther from the epicenter than for the calibration earthquakes used to define the Honshu model. In fact, the efficient propagation of energy from the 1855 Ansei Edo source to distant sites is fit by the subducting-plate model for events at 30- and 70-km depth (Fig. 18a and 18b). That is, Usami's (1996) intensity assignments are more consistent with subduction-plate sources at 30-70 km depth than with a shallow crustal source in the Eurasian plate. Shallow-to-intermediate depth intraslab events occur near the top surfaces of descending plates (Kirby *et al.*, 1996), so an intraslab PHS plate source (Nakamura *et al.*, 2003) and a PHS-Eurasian interplate source are difficult to discriminate using intensity data. The depth of the PAC-PHS contact surface is greater than 60 km beneath Tokyo (Noguchi, 2002) and slip in interplate events does not extend to depths greater than about 50 km (Kirby *et al.*, 1996), so the 1855 Ansei Edo earthquake could not have been a PAC-PHS interplate event. However, a source near the top of the PAC plate (a PAC intraslab source), as suggested by Hikita and Kudo (2001) and as modeled in Fig. 18b, cannot be ruled out using the intensity data.

Consider the 1855 Ansei Edo earthquake as an $M_{jMA}7.2$ PHS-Eurasian interplate event at 30 km depth. Usami's (1996) intensity assignments constrain the epicenter location to within a few tens of kilometers of the intensity center (Fig. 19). Furthermore, possible epicenter locations (95% confidence level) are constrained to the region of the PHS plate to the northeast of the main slip regions of the Great 1923 Kanto earthquake (Fig. 20). If on the PHS-Eurasian plate interface, the 1855 Ansei Edo event could plausibly have ruptured an adjacent downdip section of the subducting PHS plate as suggested by Ohtake (1980) and Kasahara (1985). The expected

faulting area of an M_{JMA} 7.2 shallow interplate earthquake in Japan is 3,165 km² (Sato, 1989). A circular area A of 3,165 km² (shaded red), centered on the intensity center obtained for the 1855 Ansei Edo event, is plotted in Figure 20 relative to Nyst *et al.*'s (in preparation) rupture area for the M_{JMA} 7.9 Great 1923 Kanto earthquake. If the 1855 Ansei Edo and Great 1923 Kanto earthquakes were both PHS-Eurasian interplate events, the 1855 Ansei Edo event probably ruptured adjacent to and down dip of the Great 1923 Kanto earthquake, as suggested by Ohtake (1980) and Kasahara (1985).

The Kanto region was particularly active in the forty years before 1923 (Okada, 2001), and the inferred rupture area of the 1855 Ansei Edo event is near a gap in a NE-SW trending band of $M > 6.0$, $h < 60$ km, 1883-1923 epicenters (Fig. 21). The inferred slip area of the 1855 earthquake appears to complement the band of epicenters of the 1883-1923 events, suggesting the possibility that the PHS-Eurasian plate interface, seismically quiet since 1923, was seismically active in the 75 years before the Great 1923 Kanto earthquake.

Hikita and Kudo (2001) suggested that the 1855 Ansei Edo earthquake was an M_{JMA} 7.4 PAC-plate intraslab event at about 70 km depth, the depth of the PAC-PHS contact zone at the intensity center (Noguchi, 2002). The subducting-plate model is consistent with an M_{JMA} 6.9 PAC-plate intraslab event at 80 km depth (Fig. 13e) and with an M_{JMA} 6.7 PHS-plate intraslab event at 47 km depth (Fig. 13f) so it is reasonable that it is appropriate for a 70-km-deep PAC-plate intraslab earthquake beneath Tokyo. The intensity center is centered on Noguchi's (2002) PAC-PHS contact surface. Historical data suggest, however, that the 1855 Ansei Edo earthquake was preceded by alterations in groundwater, springs, and by "ground rumbling," and seventy-eight aftershocks were felt in Tokyo in the month immediately following the earthquake (Usami, 1996). Aftershocks of intermediate-depth intraslab events are rare. For example, there were no aftershocks following the large intraslab events at 60-70 km depth beneath Puget Sound, Washington state, in 1949 (magnitude 4.5 detection threshold) and 1965 (magnitude 2.5 detection threshold) (Ludwin *et al.* 1991). Only four small aftershocks (coda-length magnitude detection threshold 1.0) occurred after the M_w 6.8 2001 Nisqually intraslab earthquake at 52 km depth (Pacific Northwest Seismograph Network, 2004). The more vigorous aftershock sequence following the 1855 Ansei Edo earthquake renders a PAC-plate intraslab source (Hikita and

Kudo, 2001) unlikely. The aftershock activity supports a shallower source, but the absence of reports of surface faulting, which would certainly be expected for a large shallow crustal event, do not support the shallow crustal source suggested by Furumura (2003). Finally, an order of magnitude more aftershocks were felt after the shallow crustal 1994 $M_{JMA}7.3$ Kobe earthquake (JMA, 2004), suggesting a somewhat deeper source for the 1855 Ansei Edo event.

Is the aftershock activity following the 1855 Ansei Edo event consistent with an $M_{JMA}7.2$ PHS-Eurasian interplate source? The intraslab events in Puget Sound cited above occurred at depths of 60-70 km, whereas the proposed PHS-Eurasian interplate source (or a PHS intraslab source) would be somewhat deeper than 30 km, the downdip extent of rupture during the Great 1923 Kanto earthquake (*e.g.*, Nyst *et al.*, in preparation). An $M_{JMA}6.7$ PHS intraslab event occurred on December 17, 1987 off Chiba at 47 km depth (Okada and Kasahara, 1990). Many aftershocks in the 20-to-45 km depth range occurred in the days after the off-Chiba main shock. However, more felt aftershocks were reported after the 1855 event than after the 1987 off-Chiba event (JMA, 2004). The aftershock activity reported after the 1855 earthquake is apparently consistent with an $M_{JMA}7.2$ PHS-Eurasian interplate source (or a PHS intraslab source) at 30-40 km depth. These sources are consistent with both the intensity data and the reported aftershocks, and other candidate seismogenic structures are not. I conclude that the 1855 Ansei Edo earthquake was an $M_{jma}7.2$ PHS-Eurasian interplate event or an $M_{jma}7.2$ PHS intraslab event. M_{JMA} is 6.9 to 7.5 at the 1σ confidence level.

Discussion

Crustal or subducting-plate event? The Honshu and subducting-plate intensity attenuation models permit the estimation of M_{JMA} for crustal earthquakes and for subduction-plate events respectively. I_{JMA} assignments of shallow crustal and subduction plate events are not markedly dissimilar at near Δ and are often overprinted at large Δ by anomalous site effects. Discrimination of depth, and causative seismogenic structure, is important because M_{jma} will be dramatically greater if a shallow crustal source rather than a subducting-plate source is assumed. However, the difference in inferred magnitude may imply effects that allow depth discrimination. For example, since tsunamis are reported for large offshore subduction-plate

events, the detailed record of historical tsunami occurrence may identify some historical earthquakes as subducting-plate events. Alternatively, great shallow crustal events might be identified by accounts consistent with significant surface faulting. The source of many historical events, however, will likely remain ambiguous so that alternative source location-magnitude solution pairs should be considered in seismic hazard analysis.

The comparison of intensity model predictions for the 1855 Ansei Edo earthquake shown in Figure 18 and Nakamura *et al.*'s (1994) attenuation model suggest a possible strategy for discriminating between competing seismogenic-structure hypotheses for historical earthquakes. The high-velocity high-Q PAC and PHS plates propagate shaking more efficiently than the Eurasian plate, and the difference is particularly evident at Δ greater than about 200 km. The analysis of intensities near the epicenter is complicated by uncertainty in epicenter location and focal depth and intensity assignments at large Δ increasingly reflect anomalous site effects. Analysis of intensity data for focal depth necessarily must be restricted to a range of Δ that minimizes effects of uncertain source location and anomalous site effects.

In this study, I consider a least-squares linear fit of the difference between observed intensity and predicted intensity for intensity assignments at $100 \leq \Delta \leq 400$ km (Fig. 22). If the attenuation model is correct and there are no errors in intensity assignments or uncorrected site effects, then the slope of the linear fit should be zero. If the slope is significantly different from zero, then at least one of the above assumptions is incorrect. Slopes for the four shallow test events (#T1-T4) are listed in Table 6. The slopes are greater than zero using the model for a shallow source in the Eurasian plate, and not very different from zero using the model for an intermediate depth source on a subduction plate (Figs. 22a and 22c). If site corrections are used, the slopes for events #T1 and T2 are not very different from zero for the model for a shallow source in the Eurasian plate and less than zero using the model for an intermediate depth source on a subduction plate (Figs. 22b and 22d). An incorrect inference of source depth and location is obtained without site corrections, and a correct inference is obtained when site corrections are applied. There are no intensity assignments at $\Delta > 161$ km for the 1989 M_{JMA} 5.5 (#T4) event so that meaningful slopes cannot be calculated for $100 \leq \Delta \leq 400$ km. The slopes for the shallow 1941 (#T3) event, with and without site corrections, suggest, incorrectly, that the source was an

intermediate depth subduction plate event. Note that there are no intensity assignments at $260 < \Delta < 400$ km for the 1941 event so perhaps the incorrect depth inference can be attributed to lack of intensity assignments in a critical distance range. A similar analysis for the Great 1923 Kanto earthquake is shown in Figure 22e. The correct inference for depth and source region (a subduction plate source) is obtained for the Great 1923 Kanto event (site corrections are not available). Note that the distribution and slopes obtained without site corrections for events #T1, T2, and the Great 1923 Kanto event are similar.

Reliable discrimination of shallow crustal and subducting-plate historical earthquakes using intensity assignments may not be possible. Anomalous site effects tend to mask the depth signature, consistent with Furumura's (2003) observation that intensity assignments near Tokyo are controlled by site effects. Intensity assignments sampling both near and far Δ and site corrections are apparently necessary, but may not be sufficient, to infer source depth and causative seismogenic structure for historical earthquakes. For the 1855 Ansei Edo earthquake for which many intensity assignments, but no site corrections, are available (Fig. 22f), slopes are greater than zero for the three candidate sources. Slopes calculated for Usami's (1996) intensity assignments without site corrections are not consistent with any of the models considered.

Hazard Estimates for Subduction Interface Events –Other Plates. PAC and PHS plate earthquakes cause significant damage at distant sites (Fig. 13). In contrast, damage from comparable-size crustal earthquakes does not extend much beyond the epicentral region. The old, cold high-Q high-velocity subducting PAC and PHS plates serve as waveguides that propagate strong shaking with little attenuation (Nakamura *et al.*, 1994). While the evidence for anomalous damage from earthquakes on old, cold subduction plates is clear, a comparable waveguide effect may not occur for earthquakes on younger, hotter subduction plates. For example, infrequent great earthquakes occur on the currently aseismic Cascadia subduction zone along the Pacific Northwest coast of the United States (Atwater *et al.*, 1999). Although the extent of damaging ground motions from the next great Cascadia subduction event cannot be calibrated empirically using intensity data from Cascadia earthquakes, a Cascadia waveguide effect comparable to that observed for subducting-plate earthquakes in Japan should be evaluated.

Conclusions

Japan Meteorological Agency magnitudes M_{JMA} and intensity assignments I_{JMA} for earthquakes with instrumental epicenters are used to develop intensity attenuation models that can be used with Bakun and Wentworth's (1997) intensity analysis to estimate magnitudes and source locations of historical earthquakes in Japan.

1. I_{JMA} for fourteen $5.2 \leq M_{JMA} \leq 7.0$ shallow calibration events within about 300 km of Tokyo are used to derive the Honshu intensity attenuation model. The predicted intensity is equal to $-1.89 + 1.42M_{JMA} - 0.00887\Delta_h - 1.66\log\Delta_h$, where M_{JMA} is the JMA magnitude, $\Delta_h = (\Delta^2 + h^2)^{1/2}$, and Δ and h are epicentral distance and focal depth (km), respectively. The Honshu model was tested using thirty-six $5.5 \leq M_{JMA} \leq 7.3$ shallow crustal earthquakes. It is applicable for shallow crustal earthquakes throughout Japan, but regional variations must be accounted for in the estimation of magnitude.

2. Confidence contours for source locations developed for Modified Mercalli intensities and earthquakes in California are not appropriate for JMA intensities. Bootstrap re-sampling tests can be used to define confidence contours in location for earthquakes in Japan. Six of eight epicenters of test events considered lie within 1σ contours defined to include 67% of the bootstrap intensity center relocations.

3. The intensity magnitude M_{jma} is an unbiased estimate of M_{JMA} and the 1σ uncertainty in M_{JMA} using M_{jma} is $\pm 0.20-0.25 M_{JMA}$ units.

4. M_{jma} for 1997-2000 events agree with M_{JMA} , suggesting that the traditional and post-April 1996 instrument-based I_{JMA} assignments are generally consistent.

5. M_{jma} is less than M_{JMA} for three earthquakes located near the magmatic intrusion associated with the phreatic eruptions of Miyakejima in 2000, for the 23 January 1975 earthquake located on the northern rim of Mt. Aso caldera in Kyushu, and for the 3 September 1998 earthquake that

was triggered by inflation of Mt. Iwate in northern Japan, consistent with strong attenuation of 1-10Hz shear energy in hot, fractured near-source magmatic rock, and/or with relatively low frequency near-volcano earthquake sources.

6. I_{JMA} for events on the subducting Pacific and Philippine Sea plates are greater than for comparable-size shallow crustal earthquakes, consistent with high-Q subduction plates. Four earthquakes located near the Japan Trench were used to develop a subducting-plate intensity attenuation model, where the predicted intensity is equal to $-8.33 + 2.19M_{JMA} - 0.00550\Delta_h - 1.14\log\Delta_h$. The subduction-plate model is applicable to Pacific and Philippine Sea interplate and intraslab events.

7. The I_{JMA} assignments for the M_{JMA} 7.9 Great 1923 Kanto earthquake that occurred on the Philippine Sea-Eurasian plate interface are consistent with the subducting-plate model. Using the subducting-plate model, the location of the intensity center for the Great 1923 Kanto earthquake is 25 km north of the epicenter. The intensity magnitude M_{jma} is 7.7 and M_{JMA} is 7.3 to 8.0 at the 1σ confidence level.

8. Intensity assignments and reported aftershock activity for the 11 November 1855 Ansei Edo earthquake are consistent with an M_{JMA} 7.2 Philippine Sea-Eurasian interplate source or a M_{JMA} 7.2 Philippine Sea intraslab source. M_{JMA} is 6.9 to 7.5 at the 1σ confidence level. If the 1855 earthquake was a Philippine Sea-Eurasian interplate event, the intensity center was adjacent to and downdip of the rupture area of the Great 1923 Kanto earthquake, suggesting that the 1855 and 1923 events ruptured adjoining sections of the Philippine Sea-Eurasian plate interface.

Acknowledgments

This work would not have been possible without the encouragement and thoughtful comments of Ross Stein and Shinji Toda. Marleen Nyst, Fred Pollitz, and Takashi Furumura provided pre-publication copies of their papers. Nobuo Hamada provided valuable suggestions and files of

JMA intensity assignments. The Generic Mapping Tools software package by Wessel and Smith (1991) was used to generate many of the figures.

References

Ando, M., A fault-origin model of the great Kanto earthquake of 1923 as deduced from geodetic data, *Bull. Earthq. Res Inst.*, 49, 19-32, 1971.

Ando, M., Seismo-tectonics of the 1923 Kanto earthquake, *J. Phys. Earth*, 22, 263-277, 1974.

Atkinson, G. M., and T. C. Hanks, A high-frequency magnitude scale, *Bull. Seism. Soc. Am.*, 85, 825-833, 1995.

Atwater, B. F., B. L. Sherrod, A. R. Nelson, R. C. Bucknam, P. T. Pringle, and J. A. Boughner, Prehistoric earthquakes at Cascadia (abstract), *Seism. Res. Lett.*, 70, 210-211, 1999.

Bakun, W.H., Seismic activity of the San Francisco Bay region, *Bull. Seism. Soc. Am.*, 89, 764-784, 1999.

Bakun, W.H., Seismicity of California's north coast, *Bull. Seism. Soc. Am.*, 90, 797-812, 2000.

Bakun, W. H., and C. M. Wentworth, Estimating earthquake location and magnitude from seismic intensity data, *Bull. Seism. Soc. Am.*, 87, 1502-1521, 1997.

Bakun, W. H., and C. M. Wentworth, Erratum to Estimating earthquake location and magnitude from seismic intensity data, *Bull. Seism. Soc. Am.*, 89, 557, 1999.

Bakun, W.H., R. A. Haugerud, M.G. Hopper, and R.S. Ludwin, The December 1872 Washington state earthquake, *Bull. Seism. Soc. Am.*, 92, 3239-3258, 2002.

Bakun, W.H., and M.G. Hopper, Magnitudes and locations of the 1811-1812 New Madrid, Missouri, and the 1886 Charleston, South Carolina, earthquakes, *Bull. Seism. Soc. Am.*, 94, 64-75, 2004a.

Bakun, W.H., and M.G. Hopper, Historical Seismic Activity in the Central United States, *Seism. Res. Lett.*, 75, 564-574, 2004b.

Bakun, W. H., and O. Scotti, Regional intensity attenuation models for France and the estimation of magnitude and location of historical earthquakes, *Geophys. J. Intl.*, submitted.

Efron, B., The jackknife, the bootstrap and other resampling plans, *CBMS-NSF Regional Conference Series in Applied Mathematics, Society for Industrial and Applied Mathematics*, Philadelphia, 92pp., 1982.

Ekström, G., A. M. Dziewonski and J. H. Woodhouse, Centroid-moment tensor solutions for the 51 IASPEI selected earthquakes, 1980-1984, *Phys. Earth Planet. Int.*, 47, 62-66, 1987.

Fujiwara, O., F. Masuda, T. Sakai, T. Irizuki, and K. Fuse, Tsunami deposits in Holocene bay mud in southern Kanto region, Pacific coast of central Japan, *Sedimentary Geology*, 135, 219-230, 2000.

Furumura, T., Seismic intensity distribution and source mode of the 1855 Ansei Edo earthquake: examination by numerical simulations, 2003 (in Japanese),

Grünthal, G. (Editor), European Macroseismic Scale 1998, *Conseil de Léurope, Cahiers du Centre Européen de Géodynamique et de Séismologie*, 15, Luxembourg, 99 pp., 1998.

Hagiwara, T., Distribution of seismic intensities of the Tokyo earthquake in 1894, the Edo (old Tokyo) earthquake in 1855 and the Kanto earthquake in 1703, as estimated from ancient manuscripts, "Report of the Coordinating Committee for Earthquake Prediction" edited by Geographical Survey Institute Ministry of Construction Japan, 7, 27-31, 1972 (in Japanese).

Hanks, T. C., and H. Kanamori, A moment magnitude scale, *J. Geophys. Res.*, 84, 2348-2350, 1979.

Hikita, T., and K. Kudo, Estimation of source parameters and strong ground motions during the 1855 Ansei-Edo earthquake by the empirical Green's function method, *Journal of Architectural Institute of Japan*, 546, 63-70, 2001 (in Japanese).

Hinzen, K.-G., and M. Oemisch, Location and magnitude from seismic intensity data of recent and historic earthquakes in the northern Rhine area, central Europe, *Bull. Seism. Soc. Am.*, 91, 40-56, 2001.

Ishida, M., Geometry and relative motion of the Philippine Sea plate and the Pacific plate beneath the Kanto-Tokai District, Japan, *J. Geophys. Res.*, 97, 489-513, 1992.

Japan Meteorological Agency (JMA), Annual Seismological Bulletin, CD-ROM, 2004.

Joyner, W. B., and D. M. Boore, Methods for regression analysis of strong-motion data, *Bull. Seism. Soc. Am.*, 83, 469-487, 1993.

Kanamori, H., Faulting of the great Kanto earthquake of 1923 as revealed by seismological data, *Bull. Earthq. Res Inst.*, 49, 13-18, 1971.

Kanamori, H., The energy release in great earthquakes, *J. Geophys. Res.*, 82, 2981-2987, 1977.

Kanamori, H. and C. R. Allen, Earthquake repeat times and average stress drop, *Earthquake Source Mechanics, Geophysical Monograph* 37, 227-236, 1986.

Kasahara, K., Patterns of crustal activity associated with the convergence of three plates in the Kanto-Tokai area, central Japan, *Rep. Natl. Res. Cent. Disas. Prev.* 35, 33-137, 1985 (in Japanese with English abstract).

Katsumata, A., Comparison of magnitudes estimated by the Japan Meteorological Agency with moment magnitudes for intermediate and deep earthquakes, *Bull. Seism. Soc. Am.*, 86, 832-842, 1996.

Kirby, S., E. R. Engdahl, and R. Denlinger, Intermediate-depth intraslab earthquakes and arc volcanism as physical expressions of crustal and uppermost mantle metamorphism in subducting slabs, , in *Subduction Top to Bottom*, edited by E.B. Bebout et al., pp. 195-214, AGU, Washington DC, 1996.

Kubotera, A., and T. Mitsunami, An earthquake swarm in the northern part of the Aso Caldera and migration of their foci, *Tectonophysics*, 70, 223-236, 1980.

Matsuda, T., Y. Ota, M. Ando, and N. Yonekura, Fault mechanism and recurrence time of major earthquakes in southern Kanto district, Japan, as deduced from coastal terrace data, *Geol. Soc. America Bull.*, 89, 1610-1618., 1978.

Matsu'ura, M., T. Iwasaki, Y. Suzuki, and R. Sato, Statical and dynamical study on the faulting mechanism of the 1923 Kanto earthquake, *J. Phys. Earth*, 28, 119-143, 1980.

Medvedev, S. P., W. Sponheuer, and V. Karnik, Seismic intensity scale version 1964, *Inst. Geody. Publ.*, 48, Jena, 1967.

Musson, R., Intensity and intensity scales, *New Manual of Seismological Observatory Practice (WWW edition)*, www.seismo.com/msop/nmsop/nmsop.html, 1999.

Nakamura, R., K. Shimazaki, and T. Hashida, 3-D attenuation structure beneath the Japanese Islands by tomographic inversion of seismic intensity data and predicting JMA intensity distributions in a broad area, *Journal of the Seismological Society of Japan (Zisin)*, 47, 21-32, 1994 (in Japanese).

Nakamura, M., R. Matsuura, I. Kayano, I. Karakama and A. Nishiyama, Damage of the Ansei-Edo earthquake (1855/11/11) in Edo city, *Historical Earthquake*, 18, 77-96, 2003 (in Japanese).

Nishimura, T., S. Fujiwara, M. Murakami, M. Tobita, H. Nakagawa, T. Sagiya, and T. Tada, The M6.1 earthquake triggered by volcanic inflation of Iwate volcano, northern Japan, observed by satellite radar interferometry, *Geophys. Res. Lett.*, 28, 635-638, 2001.

Noguchi, S., Earthquake clusters in the Kanto and Tokai subduction zone: Implications for modes of plate consumption, in "Seismotectonics in Convergent Plate Boundary" edited by Y. Fujinawa and Y. Yoshida, Terra Scientific Publishing Company, Tokyo, 451-467, 2002.

Nyst, M., T. Nishimura, F. F. Pollitz, and W. Thatcher, The 1923 Kanto Earthquake reevaluated using a newly augmented geodetic data set, in preparation.

Ohtake, M., An unified seismotectonic model for Kanto and Tokai regions: mechanism of shallow south Kanto earthquakes, *Bosai-kagaku-gijyutsu (NIED report)*, 41, 1-7, 1980.

Okada, Y., How soon until the next large south Kanto district earthquake?, *Earth Monthly, special issue* , 34, 94-104, 2001 (in Japanese).

Okada, Y., and K. Kasahara, Earthquake of 1987, off Chiba, central Japan and possible triggering of eastern Tokyo earthquake of 1988, *Tectonophysics*, 172, 351-364, 1990.

Parsons, T., S. Toda, R. S. Stein, A. Barka, and J. H. Dieterich, Heightened odds of large earthquakes near Istanbul: An interaction-based probability calculation, *Science*, 288, 661-665, 2000.

Pollitz, F. F., M. C. J. Nyst, T. Nishimura, and W. Thatcher, Coseismic slip distribution of the 1923 Kanto earthquake, Part II, 2005, in preparation.

Research Group for Active Faults in Japan, sheet maps and inventories, rev. ed., Univ. of Tokyo Press, Tokyo, 437pp., 1991.

Sato, R., Handbook of fault parameters for Japanese earthquakes, *Kajima Shuppan-kai*, Tokyo, 390pp, 1989.

Sipkin, S. A., Moment tensor solutions estimated using optimal filter theory for 51 selected earthquakes, 1980-1984, *Phys. Earth Planet. Int.*, 47, 67-97, 1987.

Sudo, Y., and L. S. L. Kong, Three-dimensional seismic velocity structure beneath Aso Volcano, Kyushu, Japan, *Bull. Volcanol.*, 63, 326-344, 2001.

Swiss Seismological Service, ECOS –Earthquake Catalog of Switzerland, ECOS Report to PEGASOS, Version 31.3, http://histserver.ethz.ch/publications_e.html, 2002.

Toda, S, R. S. Stein, and T. Sagiya, Evidence from the AD 2000 Izu islands swarm that stressing rate governs seismicity, *Nature* , 419, 58-61, 2002.

Usami, T., Materials for Comprehensive List of Destructive Earthquake in Japan, *Univ. of Tokyo Press*, 605pp, 1996 (in Japanese).

Utsu, T., Relation between seismic intensity, epicentral distance and magnitude Part 1. Empirical formula for shallow earthquakes in Japan excluding those occurring off the Pacific coast of eastern Japan, *Bull Earthq. Res Inst. Univ. Tokyo*, 59, 219-233, 1984.

Utsu, T., Relation between seismic intensity, epicentral distance and magnitude Part 2. Empirical formula for uppermost mantle earthquakes in Japan excluding those occurring off the Pacific coast of eastern Japan, *Bull Earthq. Res Inst. Univ. Tokyo*, 61, 551-561, 1986.

Utsu, T., Relation between seismic intensity, epicentral distance and magnitude Part 3. Empirical formula for earthquakes occurring off the Pacific coast of eastern Japan, *Bull Earthq. Res Inst. Univ. Tokyo*, 62, 289-296, 1987.

Utsu, T., Relation between seismic intensity near the epicenter, focal depth and magnitude, *Bull Earthq. Res Inst. Univ. Tokyo*, 63, 23-31, 1988.

Wald, D. J., and P. G. Somerville, Variable-slip rupture model of the great 1923 Kanto, Japan, earthquake; geodetic and body-waveform analysis, *Bull. Seism. Soc. Am.*, 85, 159-177, 1995.

Wessel, P. and W. H. F. Smith, Free software helps map and display data, *EOS*, 72, 441, 445-446, 1991.

Wood, H. O., and F. Neumann , Modified Mercalli Intensity Scale of 1931, *Bull. Seismol. Soc. Am.*, 21, 277-283, 1931.

Figure captions

Figure 1. *a)* Calibration earthquakes (C1-C14 in Table 1) and test earthquakes (T1-T4 in Table 2 and T5-T37 in Table 4) plotted as circles and triangles respectively. The off-Izu area is enlarged in the *inset*. *b)* ($M_{JMA} - M_I$) for the calibration and test events. Colors identify events referenced in subsequent figures.

Figure 2. I_{JMA} for the 14 calibration earthquakes.

Figure 3. I_{JMA} residuals for the 36 median Δ_h listed in Table 1. I_{pred} were calculated using (3).

Figure 4. I_{JMA} assignments (circles) versus Δ_h for 4 calibration events. The open squares are those median Δ_h used in the regression. The Honshu model is plotted for the M_{JMA} for each event.

Figure 5. I_{JMA} assignments (circles) versus Δ_h for the 4 test events (Table 2). The open squares are median Δ_h calculated using the median Δ_h criteria described for the calibration events. The Honshu model is plotted for the M_{JMA} for that event.

Figure 6. M_{jma} versus M_{JMA} for the 14 calibration events (solid dots) and the 4 test events (open squares). *(a)* M_{jma} evaluated for a location at the epicenter without site corrections; *(b)* M_{jma} evaluated at the intensity center without site corrections; *(c)* M_{jma} evaluated at the intensity center with site corrections.

Figure 7. Four test earthquakes assuming a depth of 5 km and using empirical intensity site corrections. Black circles are sites with I_{JMA} assignments; $VI \leq (I_{JMA} - \text{site correction}) < VII$ are plotted as I_{JMA} VI, and so on. The contours of M_{jma} (dashed red lines) are the best estimates of M_{JMA} from the I_{JMA} assignments for assumed epicenters on that contour. The rms [M_{jma}] contours corresponding to the 67% (innermost contour) and 95% confidence levels (outermost contour) for location from Bakun and Wentworth (1999) are shown as solid green lines.

Figure 8. Bootstrap resampling tests for the 4 test earthquakes shown in figure 7. (*left*) without site corrections; (*right*) with site corrections. Black circles are 1,000 bootstrap resampling intensity centers. The green contours are 67% and 95% confidence location contours from Bakun and Wentworth (1999) (see Fig. 7 caption). The intensity centers and epicenters are shown as green triangles and red stars, respectively. The red contours are those rms [M_{jma}] contours that enclose about 67% of the bootstrap resampling intensity centers.

Figure 9. Histograms of M_{jma} for the bootstrap resampling intensity centers within the 1σ location (red) contours in figure 8 (left).

Figure 10. I_{JMA} assignments (circles) versus Δ_h for six test events from other regions (locations shown as red triangles in figure 1b).

Figure 11. Test earthquakes shown in figure 10 assuming a depth of 5 km (without site corrections). Black circles are sites with I_{JMA} assignments. The contours of M_{jma} (dashed red lines) are the best estimates of M_{JMA} from the I_{JMA} assignments for assumed epicenters on that contour. The rms [M_{jma}] contours corresponding to the 67% (innermost contour) and 95% confidence levels (outermost contour) for location from Bakun and Wentworth (1999) are shown as solid green lines.

Figure 12. I_{JMA} for five 1997-2000 shallow test events located near the Izu volcanic islands (locations shown as red triangles in the inset of figure 1b): *a*) events near Toda *et al.*'s (2002) magmatic dyke. *b*) events not near Toda *et al.*'s (2002) magmatic dyke.

Figure 13. I_{JMA} assignments (circles) versus Δ_h for PAC plate events. *a*)-*d*): four shallow PAC plate events near the Japan Trench (locations shown as solid green triangles in figure 1b). The open squares are those median Δ_h used to derive the subducting-plate model. *e*)-*f*) intermediate depth PAC and PHS intraplate events (locations shown as open green triangles in figure 1b). The subducting-plate model is plotted for the M_{JMA} for each event.

Figure 14. I_{JMA} assignments (circles) versus Δ_h for the Great 1923 Kanto earthquake. The open squares are median Δ_h selected using the median Δ_h criteria described for the calibration events. The Honshu and subducting-plate models for an $M_{JMA} 7.7$ source at 5 km and 23 km depth respectively are shown for comparison.

Figure 15. The Great 1923 Kanto earthquake assuming a depth of 23 km and the subducting-plate model. The intensity center and the JMA epicenter are shown as a green triangle and star respectively. I_{JMA} IV, V, and VI assignments were used. Site corrections were not used. See caption of Fig. 11.

Figure 16. Bootstrap re-sampling test for the 1 September 1923 Kanto earthquake ($h = 23$ km, the subducting-plate model, no site corrections). I_{JMA} IV, V, and VI assignments were used. The intensity center and the JMA epicenter are shown as a red triangle and star, respectively. The offshore bootstrap locations lie on the southeast perimeter of the rectangular grid search region. See caption for Fig. 8.

Figure 17. The 11 November 1855 Ansei Edo earthquake. *a)* For a source on the PHS-Eurasian interface ($h = 30$ km, the subducting-plate model); *b)* For a PAC intraslab source ($h = 70$ km, the subducting-plate model); *c)* For a shallow crustal source ($h = 5$ km, the Honshu model). The intensity center is shown as a green triangle. Site corrections were not used. See caption of Fig. 11.

Figure 18. Usami's (1996) intensity assignments (circles) versus Δ_h for the 11 November 1855 Ansei Edo earthquake. The open squares are median Δ_h selected using the median Δ_h criteria described for the calibration events. The lines are intensity attenuation models: *a)* subducting-plate model, $M_{JMA} 7.2$ event at $h=30$ km (PHS-Eurasian interplate event); *b)* subducting-plate model, $M_{JMA} 7.4$ event at $h=70$ km (PAC intraslab event); *c)* Honshu model, $M_{JMA} 7.7$ event at $h=5$ km (shallow crustal source).

Figure 19. Bootstrap re-sampling test for the 11 November 1855 Ansei Edo earthquake for a PHS-Eurasian interplate source ($h = 30$ km, the subducting-plate model). Site corrections were

not used. The intensity center and Usami's (1996) epicenter are shown as solid and open green triangles respectively. The inner and outer red contours are the 67% and 95% confidence contours for location respectively (67% of the 1,000 bootstrap intensity centers are inside the inner contour and 95% are within the outer contour).

Figure 20. Intensity center (green triangle) and JMA epicenter (green star) for the Great 1923 Kanto earthquake and intensity center (red triangle) and 67% and 95% contours (red) for the 1855 Ansei Edo earthquake (for $h = 30$ km and the subducting-plate model) are shown relative to Nyst *et al.*'s (2005) uniform-slip model for the Great 1923 Kanto earthquake: the green boxes are the surface projections of two slip planes dipping to the northeast with displacement of the PHS plate relative to the Eurasian plate shown as green arrows. A circular area (shaded red), approximately appropriate for the rupture area of an $M_{JMA} 7.2$ shallow interplate event, is centered on the intensity center of the 1855 event.

Figure 21. Intensity center of the 1855 Ansei Edo earthquake (smaller thick circle) and epicenter of the Great 1923 Kanto earthquake (larger thick circle) relative to Okada's (2001) epicenters of $M_{JMA} \geq 6.0$, $h \leq 60$ km earthquakes, 1883-1923. Symbol size is proportional to M_{JMA} .

Figure 22. Fit of intensity differences to a shallow Honshu model event (solid dots) and to an intermediate-depth subducting-plate model event (open triangles). The fit for the 1855 Ansei Edo earthquake for $h = 70$ km for a subducting-plate model (open squares) is also shown in *f*). The dashed lines are least-squares linear fits of the intensity differences (observed – calculated) for $100 \leq \Delta \leq 400$ km. The slopes of the linear fits are listed in Table 6.

Table 1. Calibration Earthquakes

	Date	Hypocenter				# of Inten.	median Δ_h (km)				
		lat ($^{\circ}$ N)	long ($^{\circ}$ E)	depth (km)	M_{JMA}		Int V	Int IV	Int III	Int II	Int I
C1	17-May-30	34.90	139.13	13	5.8	12					166.5
C2	16-Sep-31	35.52	138.92	4	6.3	37			106.5	154.9	251.0
C3	26-Dec-49	36.68	139.76	9	6.4	36			124.3	153.0	226.5
C4	26-Dec-49	36.71	139.69	1	6.2	33			110.8	155.1	188.4
C5	19-Aug-61	36.11	136.70	10	7.0	50	141.3	149.7	231.4	282.9	
C6	9-Sep-69	35.78	137.07	0	6.6	59			140.4	197.3	296.3
C7	9-May-74	34.57	138.80	10	6.9	42			151.2	235.1	258.5
C8	14-Jan-78	34.77	139.25	0	7.0	50	61.5	175.7	231.2	372.7	
C9	3-Dec-78	34.88	139.18	20	5.4	21					156.4
C10	29-Jun-80	34.92	139.23	10	6.7	38			114.7	192.5	249.5
C11	22-Nov-86	34.55	139.53	15	6.0	27				128.1	203.9
C12	31-Jul-88	34.96	139.22	5	5.2	16					115.8
C13	2-Aug-88	34.95	139.20	2	5.2	16					102.0
C14	20-Feb-90	34.76	139.23	6	6.5	40	63.3	93.8	185.6	282.0	

Table 2. Test Earthquakes

ID	M _{JMA}	# of Int.	Date	lat (°N)	long (°E)	depth (km)	At Hypocenter		At Intensity Center without Site Corrections					At Intensity Center with Site Corrections					
							M _{jma} ^{††}	M _{JMA} ⁻ _{jma} ^{††}	lat (°N)	long (°E)	Δ [†] (km)	M _{jma}	M _{JMA} ⁻ _{jma}	lat (°N)	long (°E)	Δ [†] (km)	M _{jma}	M _{JMA} ⁻ _{jma}	
T1	7.3	51	25-Nov-30	35.04	138.98	1	7.27	0.03	35.40	139.02	40	7.29	0.01	35.31	138.98	30	7.21	0.09	
T2	6.9	46	27-Sep-31	36.16	139.25	3	6.99	-0.09	36.20	139.70	41	7.12	-0.22	35.98	138.7	52	6.95	-0.04	
T3	6.1	25	15-Jul-41	36.65	138.20	5	6.22	-0.12	35.93	137.97	83	6.13	-0.03	35.97	137.9	80	6.20	-0.10	
T4	5.5	18	9-Jul-89	34.99	139.11	3	5.61	-0.11	35.08	139.335	23	5.58	-0.08	34.90	139.1	10	5.67	-0.17	
mean =								-0.07					-0.08					-0.06	
Std. Dev.=								0.07					0.10						0.11

† Distance from the Epicenter to the intensity center

†† At hypocenter with no site corrections applied.

Table 3. Calibration Earthquakes-Results†

ID	At Epicenter				Intensity Center					Intensity Center				
	without SC		with SC		without SC					(with SC)				
	M_{jma}	$M_{JMA} - M_{jma}$	M_{jma}	$M_{JMA} - M_{jma}$	lat (°N)	long (°E)	Δ^{++} (km)	$M_{jma}^{§§}$	$M_{JMA} - M_{jma}^{§§}$	lat (°N)	long (°E)	Δ^{++} (km)	$M_{jma}^§$	$M_{JMA} - M_{jma}^§$
C1	5.47	0.3	5.59	0.2	35.62	139.27	80.4	5.33	0.5	35.53	139.04	69.9	5.44	0.4
C2	6.39	-0.1	6.39	-0.1	35.57	139.15	21.2	6.41	-0.1	35.57	138.97	7.0	6.39	-0.1
C3	6.44	0.0	6.40	0.0	36.41	139.62	32.2	6.37	0.0	36.41	139.67	30.7	6.34	0.1
C4	6.11	0.1	6.12	0.1	36.66	140.37	60.8	6.29	-0.1	36.21	139.69	55.8	6.05	0.2
C5	6.95	0.1	6.85	0.2	36.52	135.30	134.0	7.41	-0.4	35.30	137.33	106.1	6.72	0.3
C6	6.78	-0.2	6.69	-0.1	35.51	137.48	48.1	6.75	-0.2	35.37	137.57	64.7	6.67	-0.1
C7	6.88	0.0	6.77	0.1	34.71	138.66	20.4	6.81	0.1	34.62	138.75	7.5	6.81	0.1
C8	7.16	-0.2	7.00	0.0	35.13	139.43	43.5	7.08	-0.1	34.72	139.07	17.3	6.99	0.0
C9	5.66	-0.3	5.71	-0.3	35.11	139.32	28.1	5.52	-0.1	35.02	139.23	15.8	5.59	-0.2
C10	6.50	0.2	6.54	0.2	35.01	139.41	19.2	6.50	0.2	34.87	139.32	9.5	6.57	0.1
C11	6.21	-0.2	6.26	-0.3	34.41	139.76	26.4	6.34	-0.3	34.41	139.58	16.0	6.34	-0.3
C12	5.41	-0.2	5.38	-0.2	35.10	139.40	22.6	5.39	-0.2	35.01	139.22	5.2	5.36	-0.2
C13	5.35	-0.1	5.38	-0.2	35.13	139.47	31.9	5.35	-0.1	35.00	139.38	17.4	5.39	-0.2
C14	6.51	0.0	6.50	0.0	33.99	138.82	93.5	6.99	-0.5	34.22	138.87	68.6	6.81	-0.3
mean =		-0.04		-0.03			47.3		-0.10			35.1		-0.02
Std. Dev.=		0.17		0.16			34.0		0.25			31.8		0.21

† Site Correction = SC

§ At the intensity center with site corrections applied.

§§ At the intensity center without site corrections applied.

++ Distance from the epicenter to the intensity center

Table 4. Additional Test Earthquakes

a) Shallow Depth

ID	Date	lat (°N)	long (°E)	depth (km)	# of		M_{jma}^{\dagger}	$M_{JMA} - M_{jma}^{\dagger}$
					M_{JMA}	I_{JMA}		
T5	17-Oct-30	36.42	136.26	10	6.3	19	6.69	-0.4
T6 [§]	23-May-38	36.65	141.58	-	7.0	53	8.21	-0.2§§
T7	6-Apr-41	34.52	131.64	2	6.2	22	6.73	-0.5
T8	5-Mar-43	35.45	134.22	2	6.2	38	6.83	-0.6
T9	10-Sep-43	35.47	134.19	0	7.2	57	7.73	-0.5
T10	11-Sep-43	35.41	133.90	5	6.2	29	6.43	-0.2
T11	13-Jan-45	34.69	137.07	8	6.8	37	6.78	0.0
T12 [§]	12-Mar-45	35.57	142.03	-	6.6	26	7.27	0.0§§
T13	15-Jun-48	33.71	135.29	0	6.7	60	7.50	-0.8
T14	28-Jun-48	36.17	136.30	0	7.1	63	7.42	-0.3
T15	27-Jul-55	33.73	134.32	10	6.5	31	6.50	0.0
T16	16-Jun-64	38.65	139.53	0	6.1	15	6.09	0.0
T17	16-Jun-64	38.64	139.24	0	6.0	12	6.09	-0.1
T18	21-Feb-68	32.02	130.72	0	6.1	19	6.31	-0.2
T19 [§]	16-May-68	40.73	143.68	-	7.9	64	9.48	0.1§§
T20 [§]	12-Jun-68	39.42	143.13	-	7.2	47	8.37	0.1§§
T21	21-Apr-69	32.15	132.12	10	6.7	34	6.73	0.0
T22	23-Jan-75	33.00	131.13	0	6.1	20	5.90	0.2
T23	4-Jun-78	35.08	132.74	0	6.1	27	6.59	-0.5
T24	26-May-83	40.76	139.38	9	6.1	13	6.46	-0.4
T25	21-Jun-83	41.26	139.00	6	7.1	28	7.48	-0.4
T26	17-Jan-95	34.60	135.04	16	7.3	93	7.68	-0.4
T27	4-Mar-97	34.95	139.17	3	5.7	70	5.36	0.3
T28	25-Jun-97	34.44	131.67	8	6.6	164	6.84	-0.2
T29	3-May-98	34.96	139.18	5	5.7	164	5.45	0.3
T30	3-Sep-98	39.80	140.91	8	6.1	118	5.62	0.5
T31	1-Jul-00	34.19	139.20	16	6.4	292	6.03	0.4
T32	9-Jul-00	34.21	139.23	15	6.1	115	5.83	0.3
T33	15-Jul-00	34.42	139.25	10	6.3	496	6.31	0.0
T34	30-Jul-00	33.97	139.41	17	6.5	512	6.62	-0.1
T35	18-Aug-00	34.19	139.24	12	6.0	109	5.45	0.6
T36	6-Oct-00	35.27	133.35	9	7.3	418	7.54	-0.2

b Intermediate Depth

T37	21-Sep-68	41.98	142.80	80	6.9	40	7.01	-0.1§§
T38	17-Dec-87	35.37	140.52	47	6.7	48	6.79	-0.1§§

[†] M_{jma} calculated using epicenters in Table 1.

[§] Shallow events located near the Japan Trench used to develop (8).

^{§§} Calculated with (8).

Table 5. The 1855 Ansei Edo Earthquake

Model	Lat (°N)	Long (°E)	M_I
Honshu model (h= 5 km)	35.54	139.95	7.7
PHS-Eurasian Interplate (h= 30 km)	35.68	139.95	7.2
PAC Intraslab (h= 70 km)	35.59	140.04	7.4
Usami (1996)	35.65	139.80	7.0-7.1

Table 6. Estimating Depth using Intensity

Event	Slope [§]		Depth Inference ^{§§}
	Honshu model	Subducting-plate model	
25 Nov 1930 (#T1) with Site Corrections	0.0054 ± 0.0013	0.0010 ± 0.0013	30 km (Subducting-plate model)
	0.0010 ± 0.0015	-0.0035 ± 0.0015	5 km (Honshu model)
27 Sept 1931 (#T2) with Site Corrections	0.0042 ± 0.0023	-0.0004 ± 0.0023	30 km (Subducting-plate model)
	-0.0011 ± 0.0014	-0.0056 ± 0.0014	5 km (Honshu model)
15 July 1941 (#T3) [†] with Site Corrections	0.0065 ± 0.0043	0.0016 ± 0.0043	30 km (Subducting-plate model)
	0.0048 ± 0.0035	-0.0001 ± 0.0035	30 km (Subducting-plate model)
9 July 1989 (#T4) ^{††}	-	-	-
Great 1923 Kanto eqk.	0.0059 ± 0.0010	-0.0014 ± 0.0010	23 km (Subducting-plate model)
1855 Ansei Edo eqk.	0.0042 ± 0.0010	0.0040 ± 0.0010	
		0.0036 ± 0.0010 ^{†††}	

[§] ($I_{JMA} - I_{PRED}$) vs. Δ for $100 \leq \Delta \leq 400$ km ($\pm 1\sigma$)

[†] No intensity assignments at $261 < \Delta < 400$ km.

^{††} No data at $\Delta > 156$ km

^{§§} Slope within 1σ of Zero

^{†††} h=70 km (PAC intraslab event)

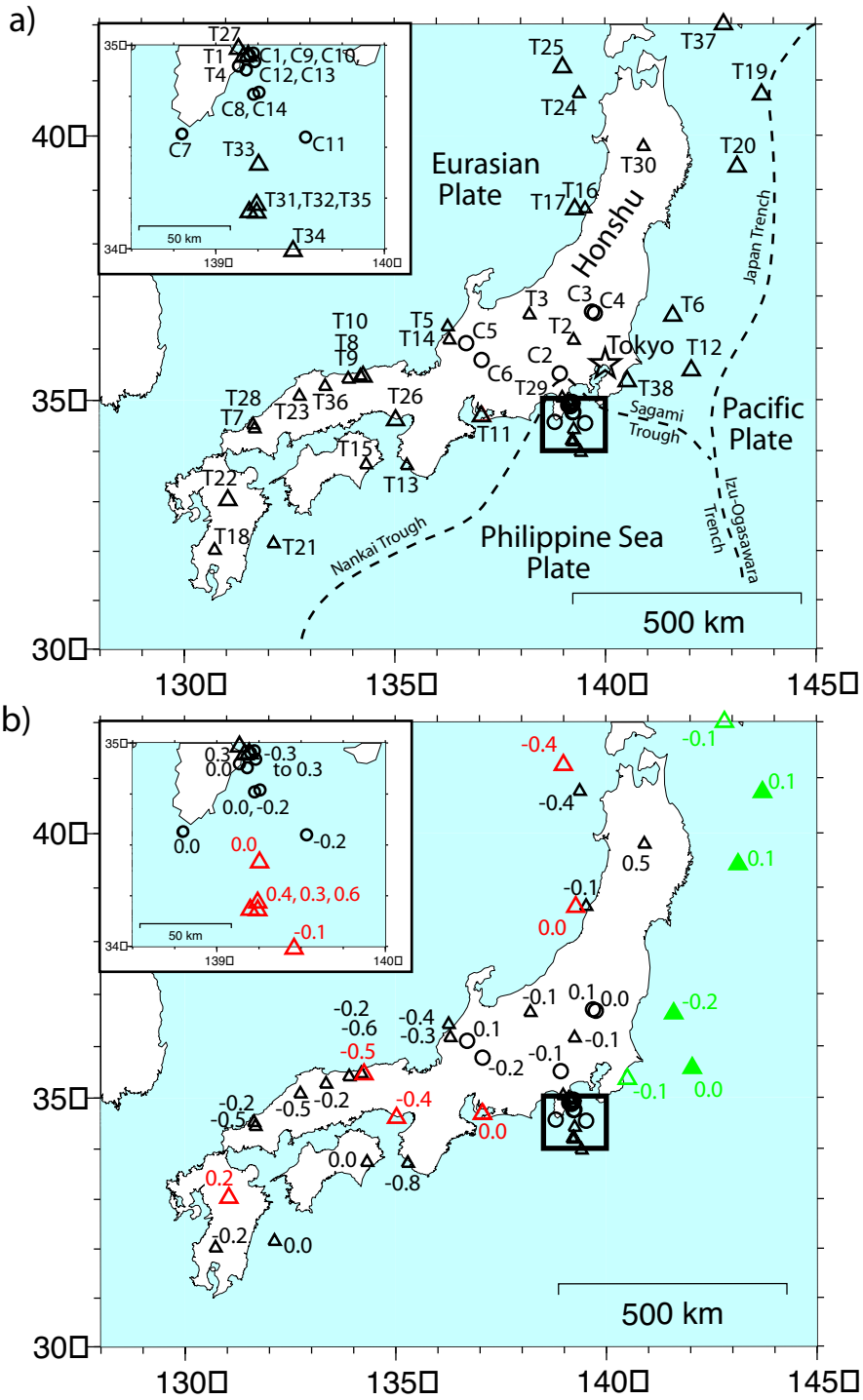


Figure 1

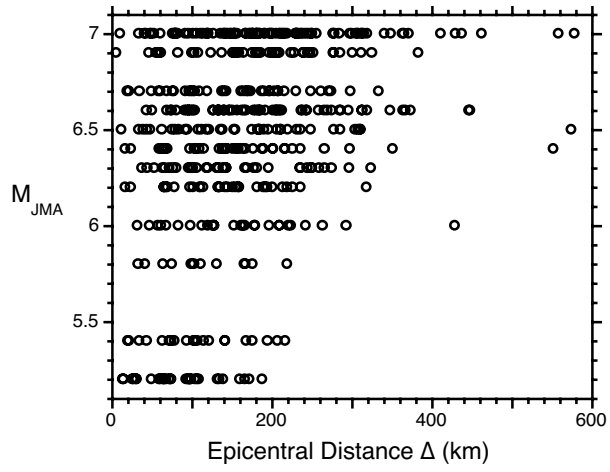


Figure 2.

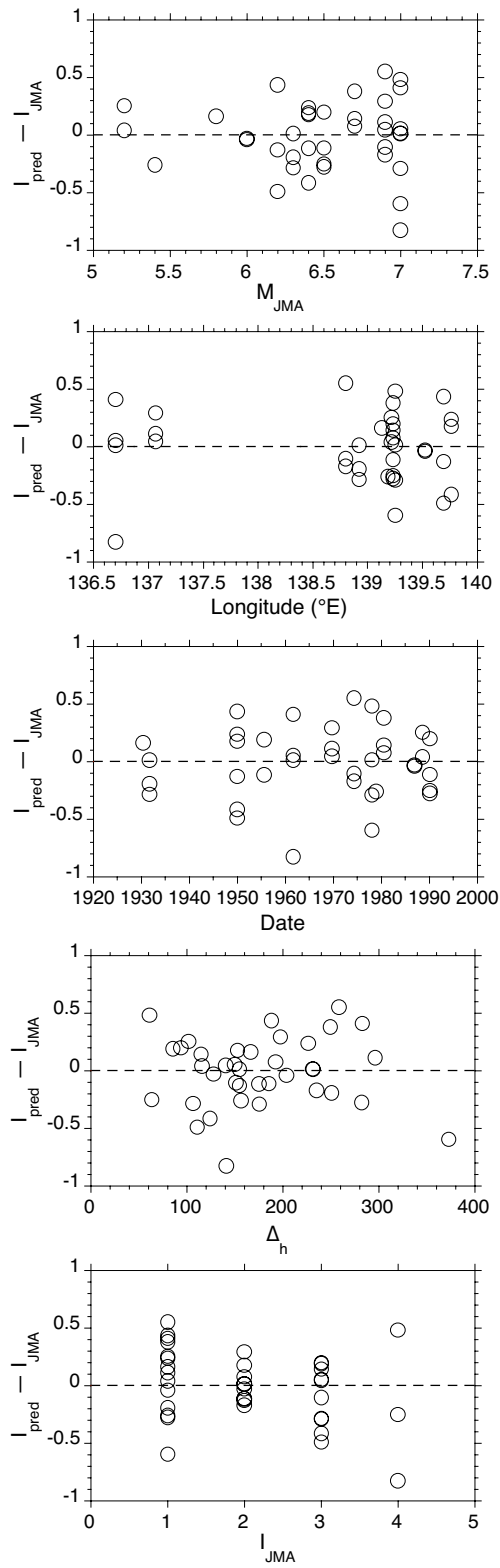


Figure 3.

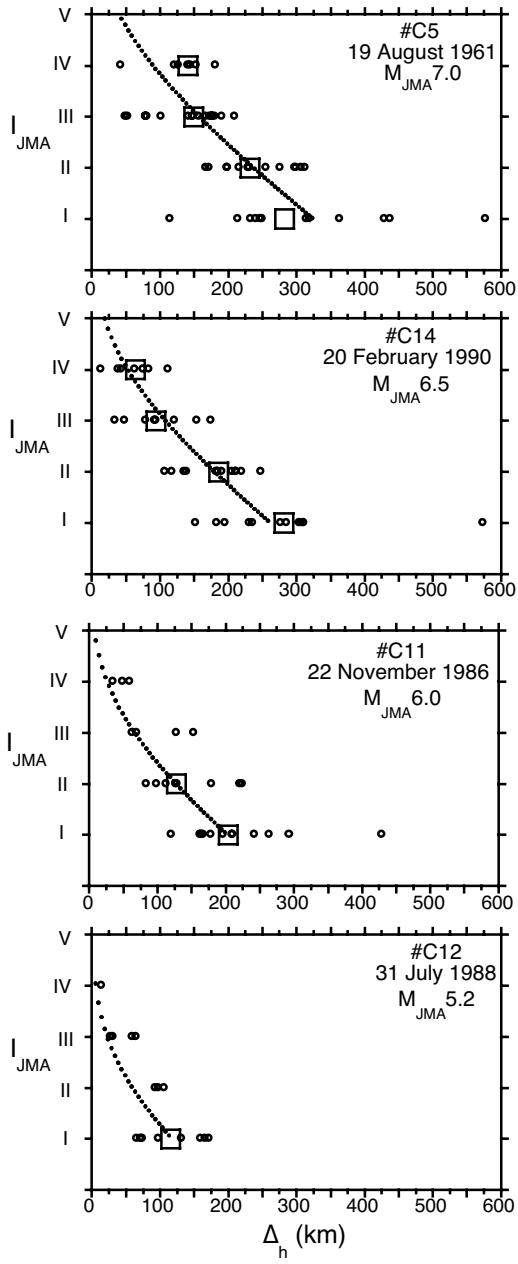


Figure 4

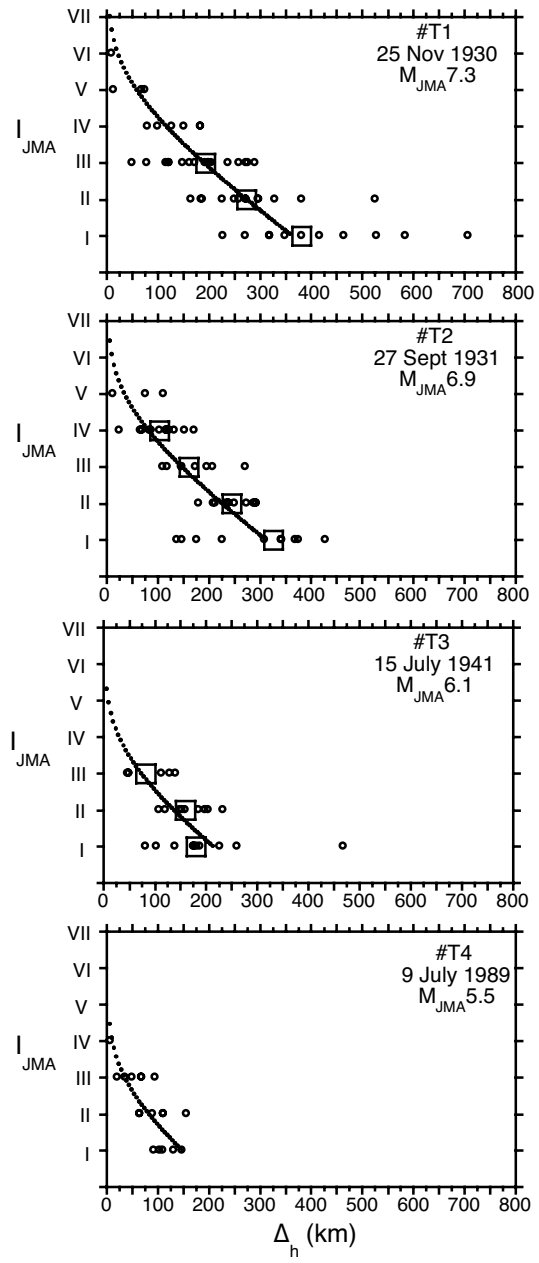


Figure 5

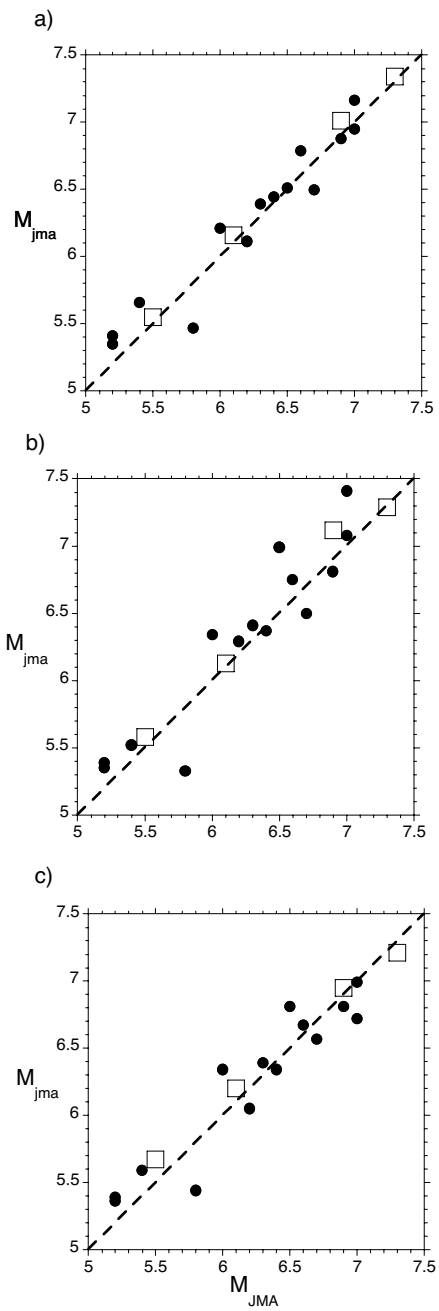


Figure 6

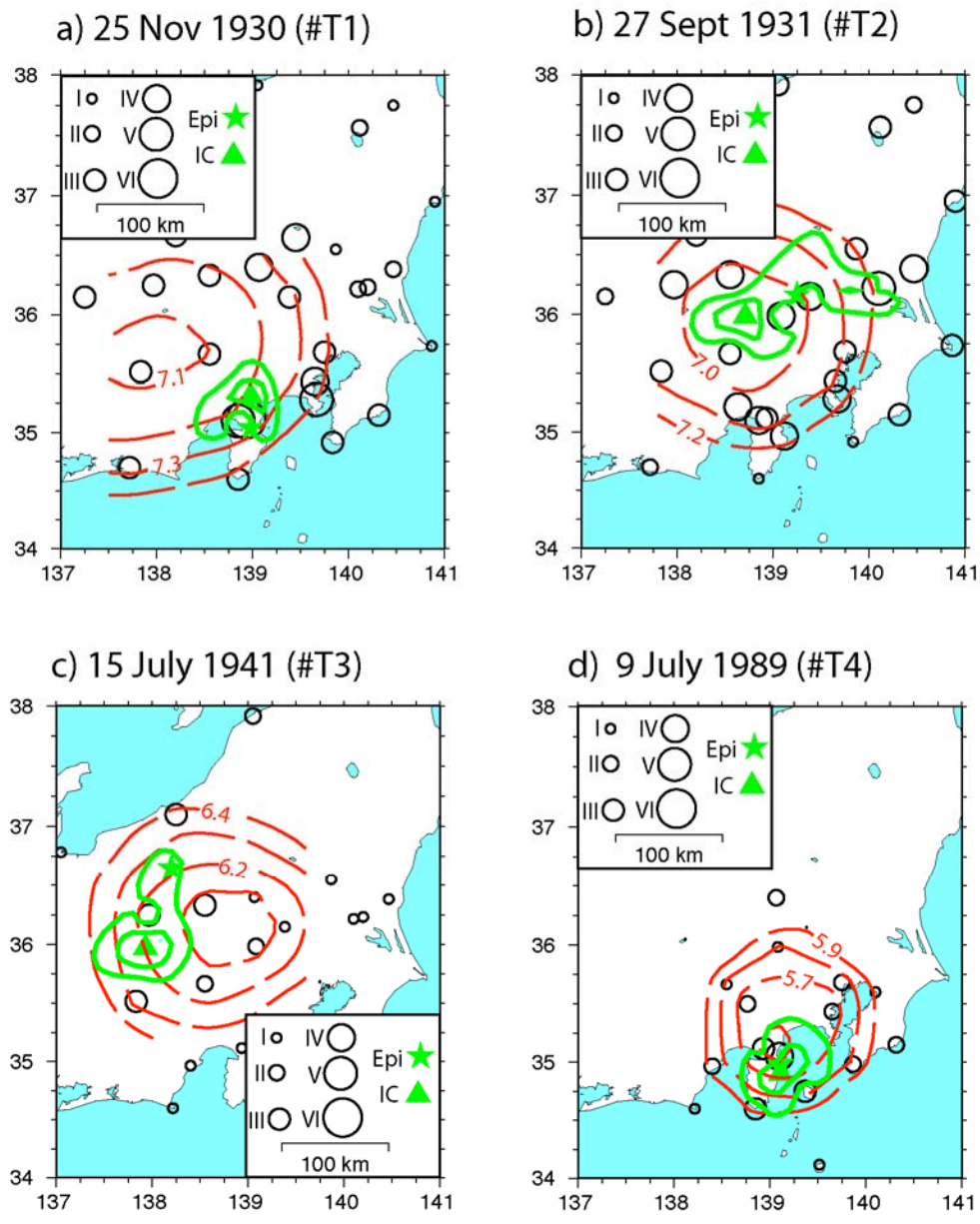


Figure 7

Without Site
Corrections

With Site
Corrections

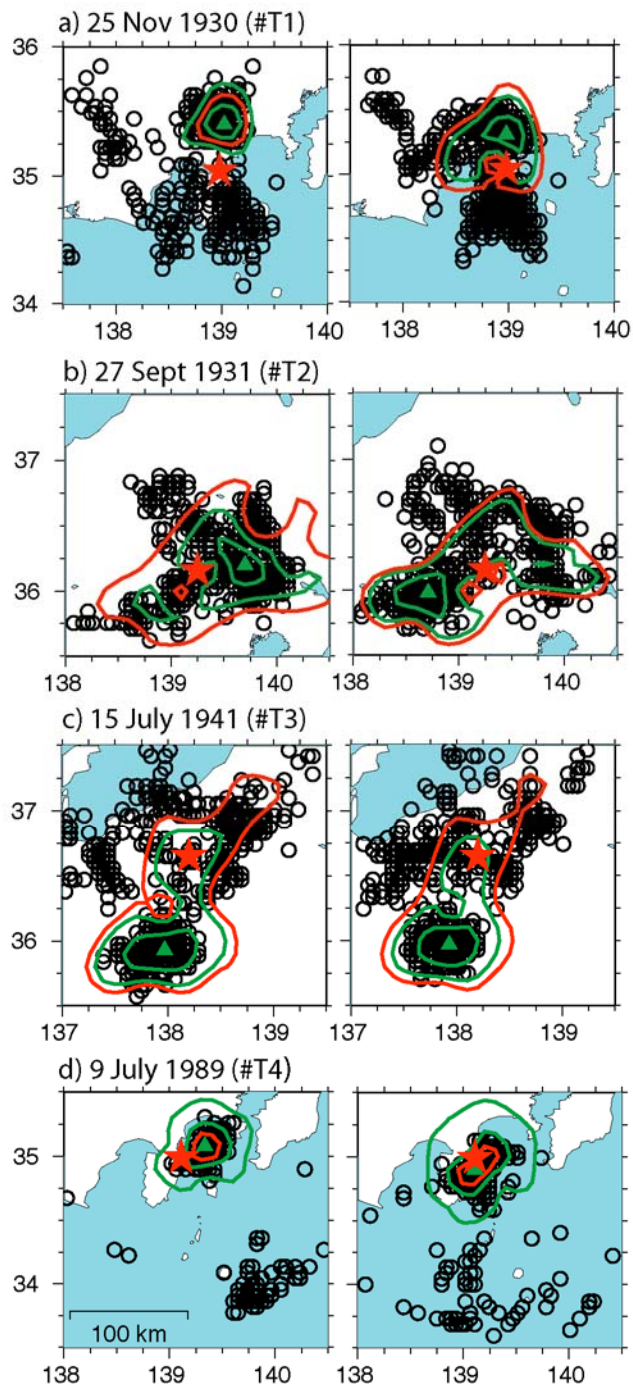
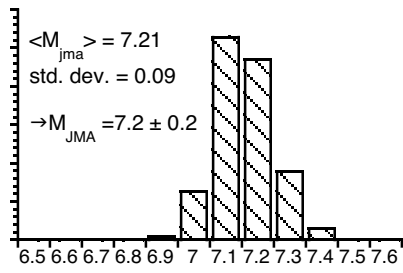
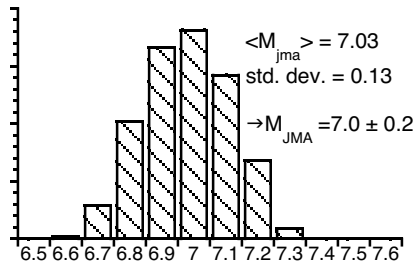


Figure 8

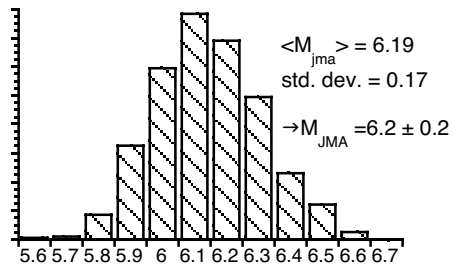
a) 25 Nov 1930 (#T1) $M_{JMA} = 7.3$



b) 27 Sept 1931 (#T2) $M_{JMA} = 6.9$



c) 15 July 1941 (#T3) $M_{JMA} = 6.1$



d) 9 July 1989 (#T4) $M_{JMA} = 5.5$

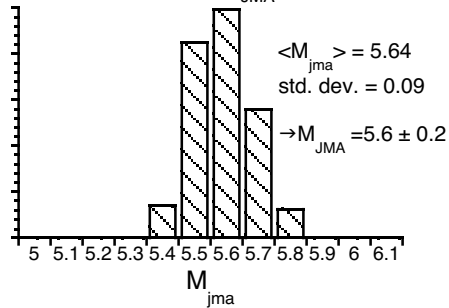


Figure 9

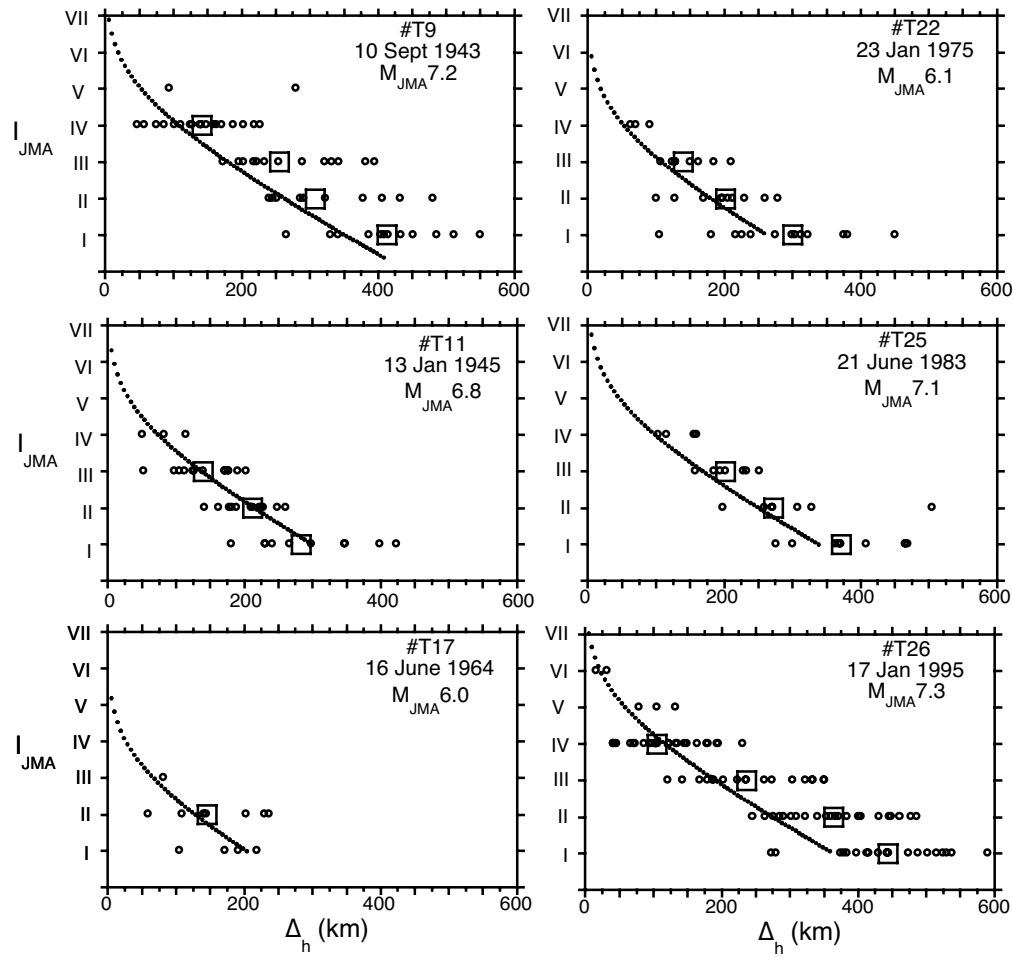


Figure 10.

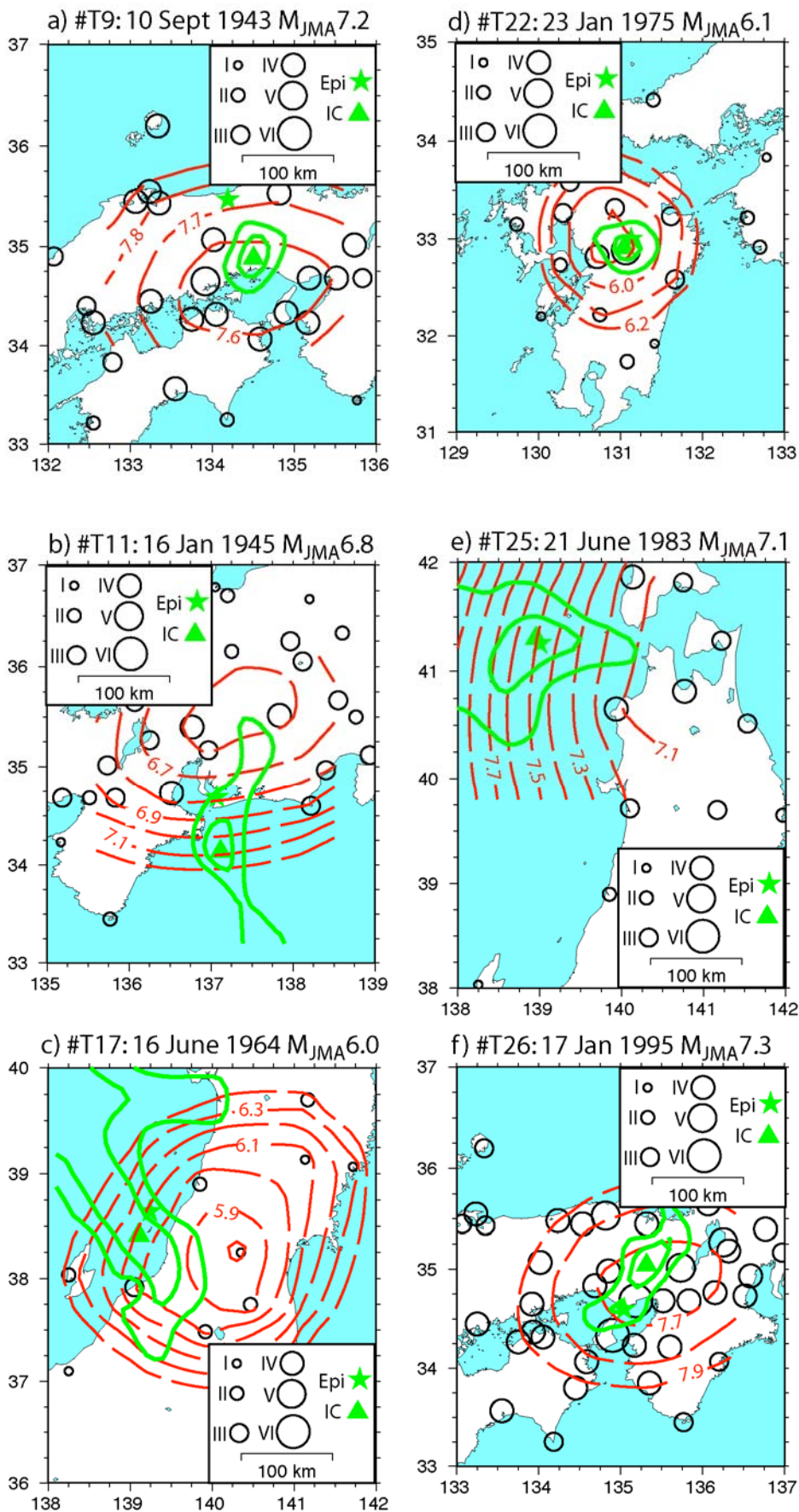


Figure 11.

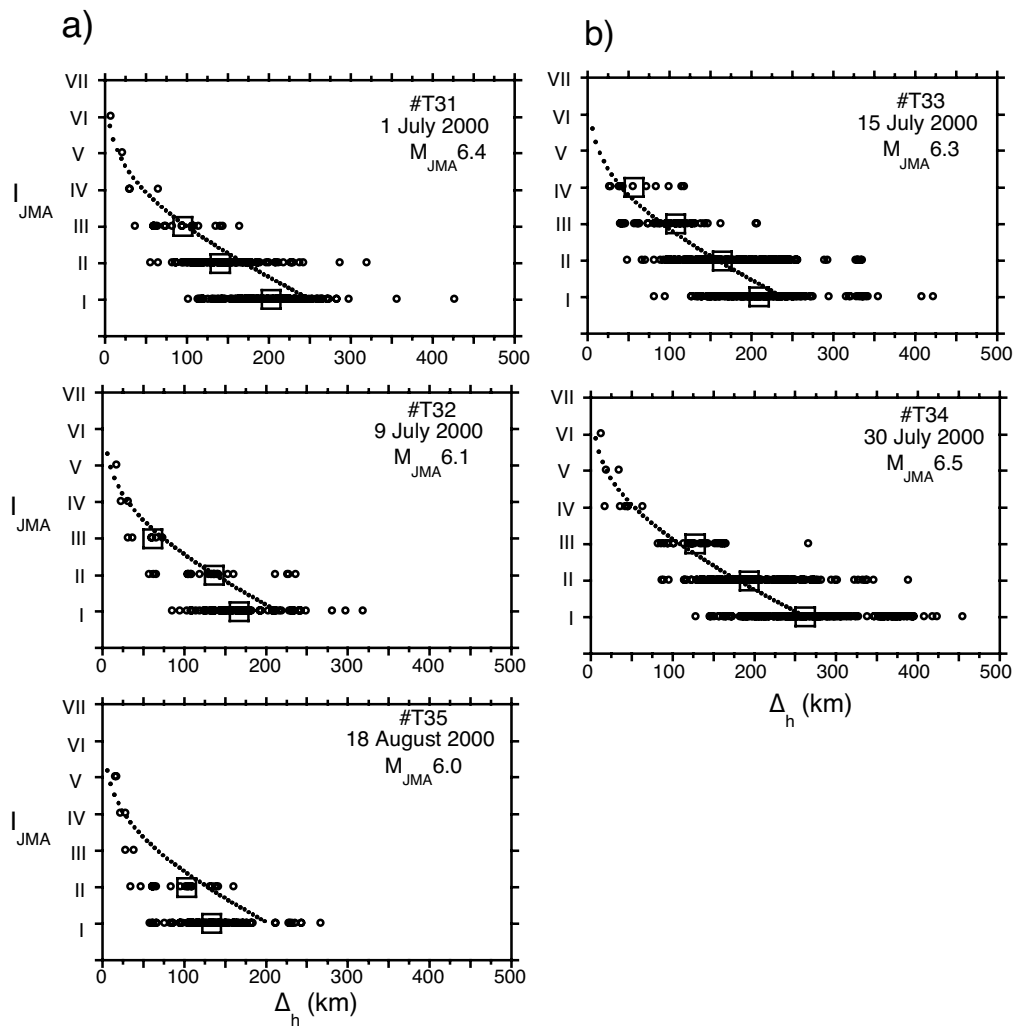


Figure 12

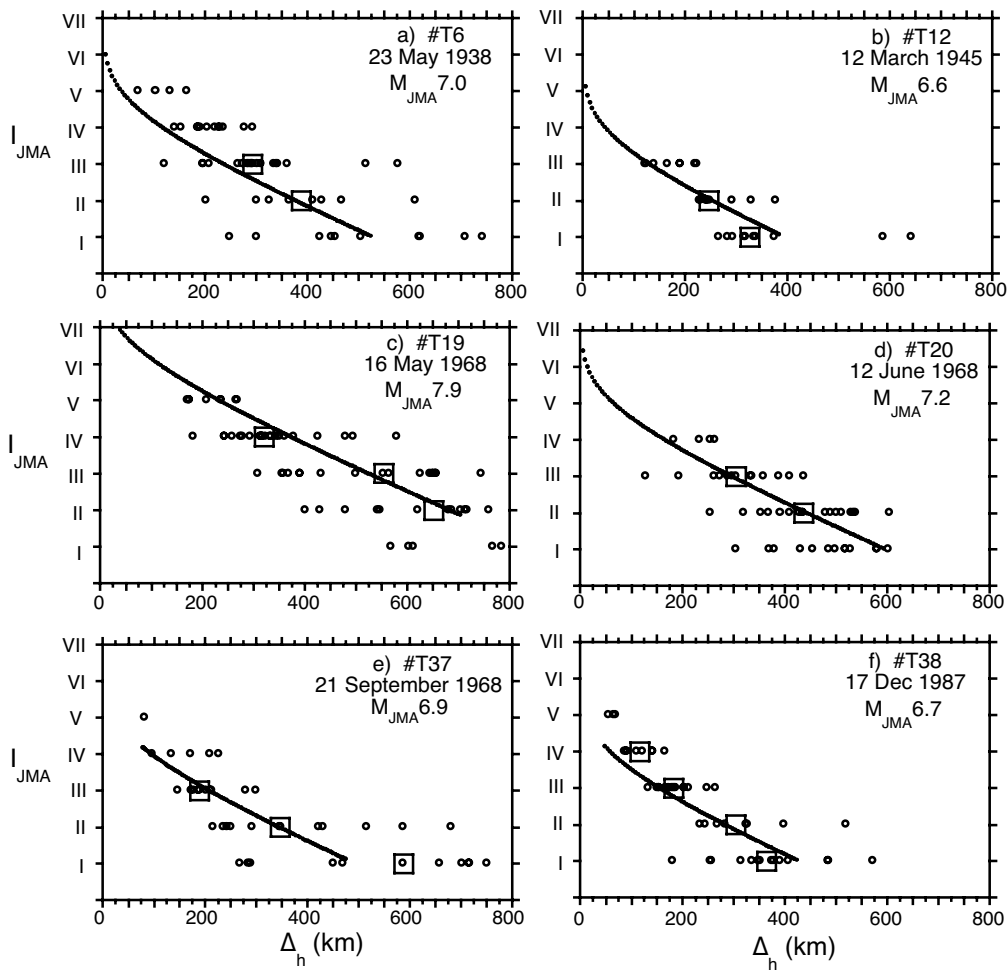


Figure 13

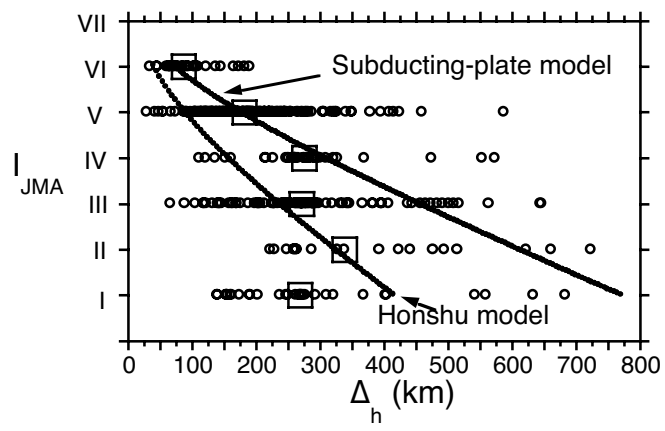


Figure 14

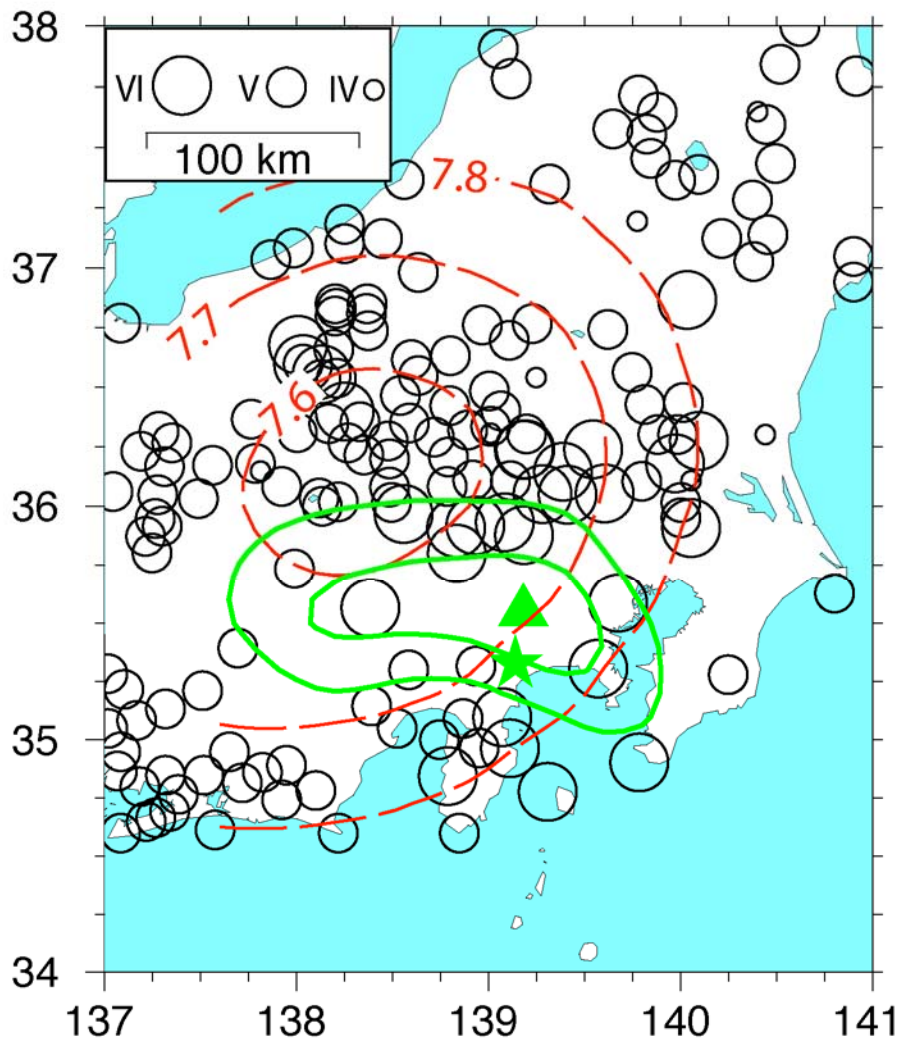


Figure 15

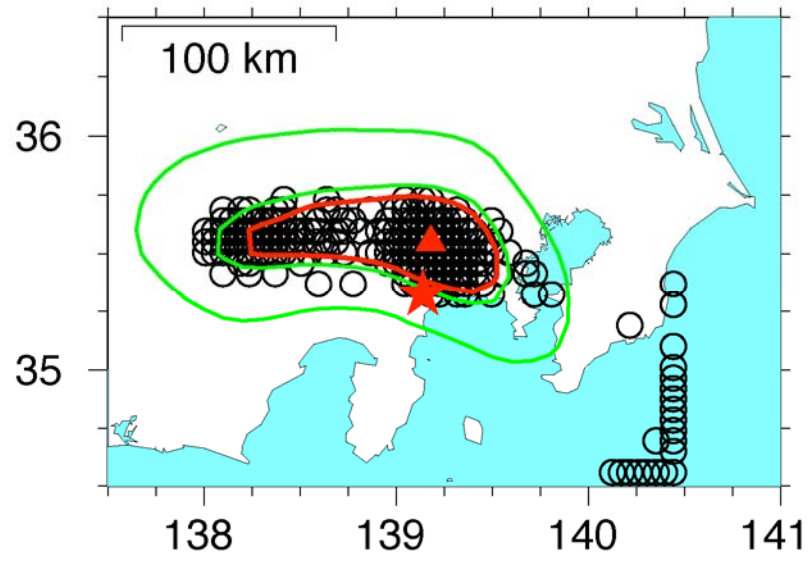


Figure 16

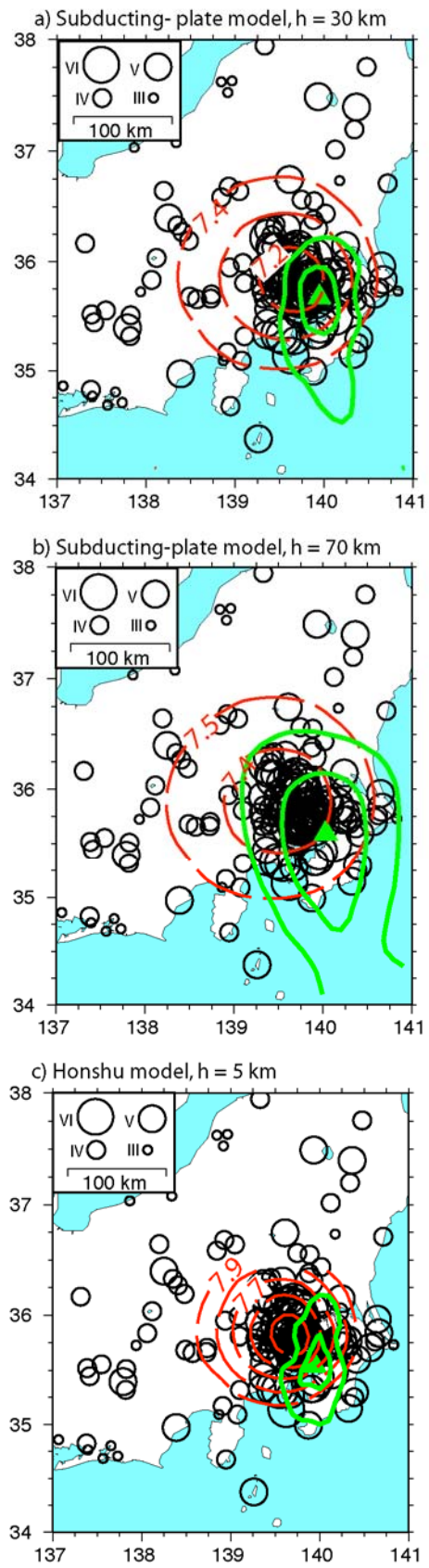


Figure 17

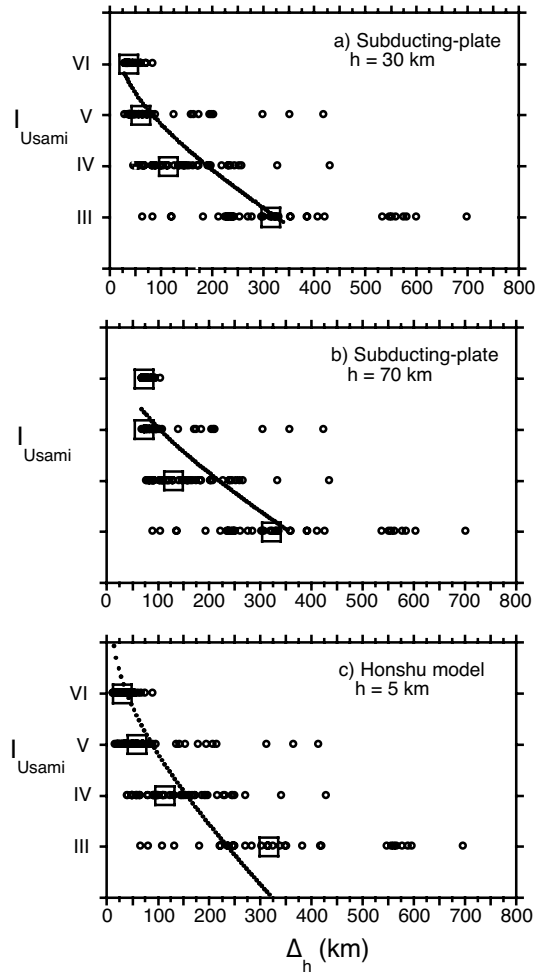


Figure 18

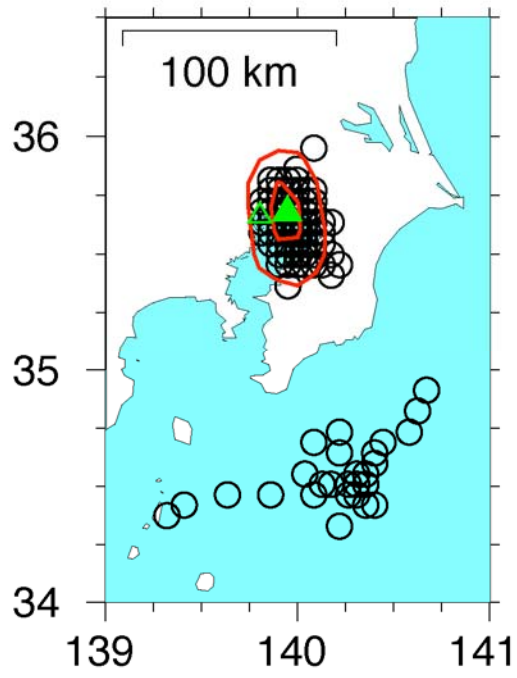


Figure 19

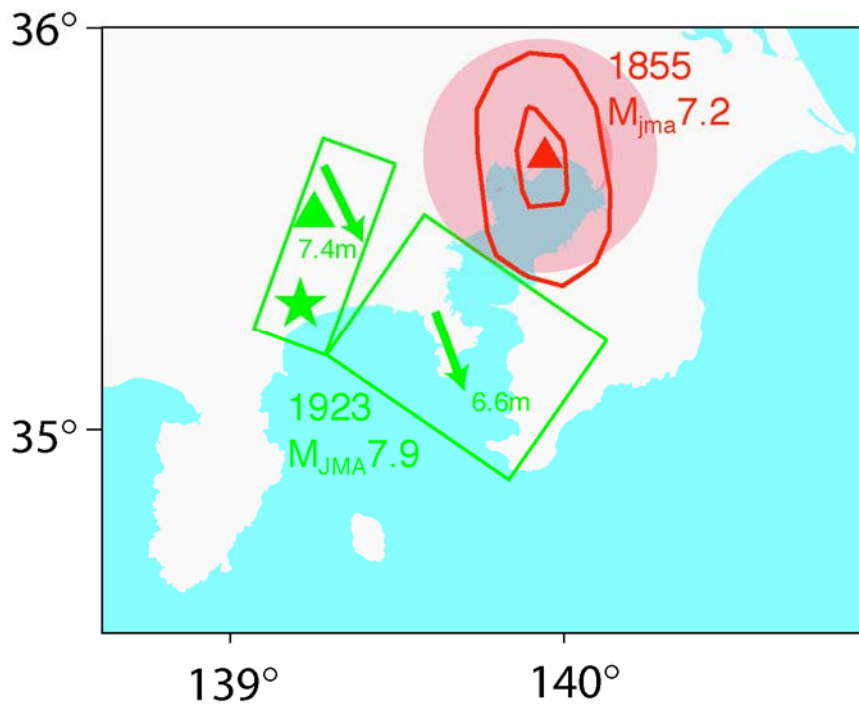


Figure 20

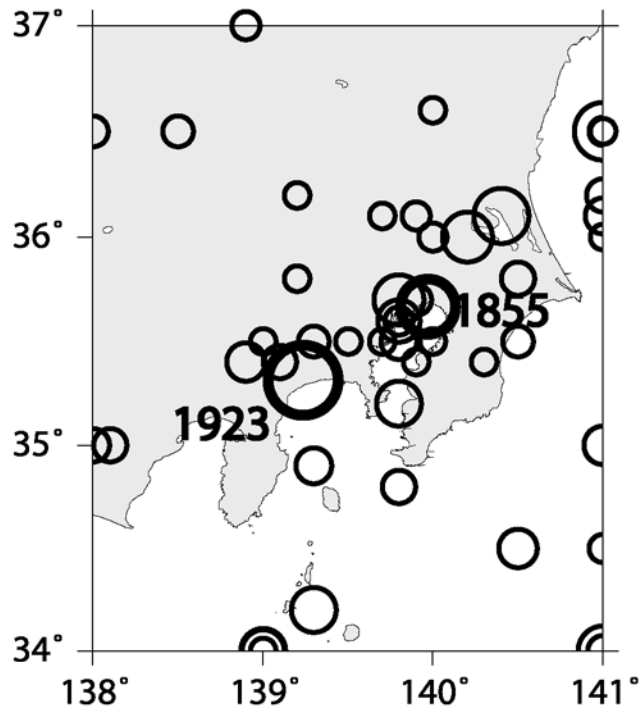


Figure 21

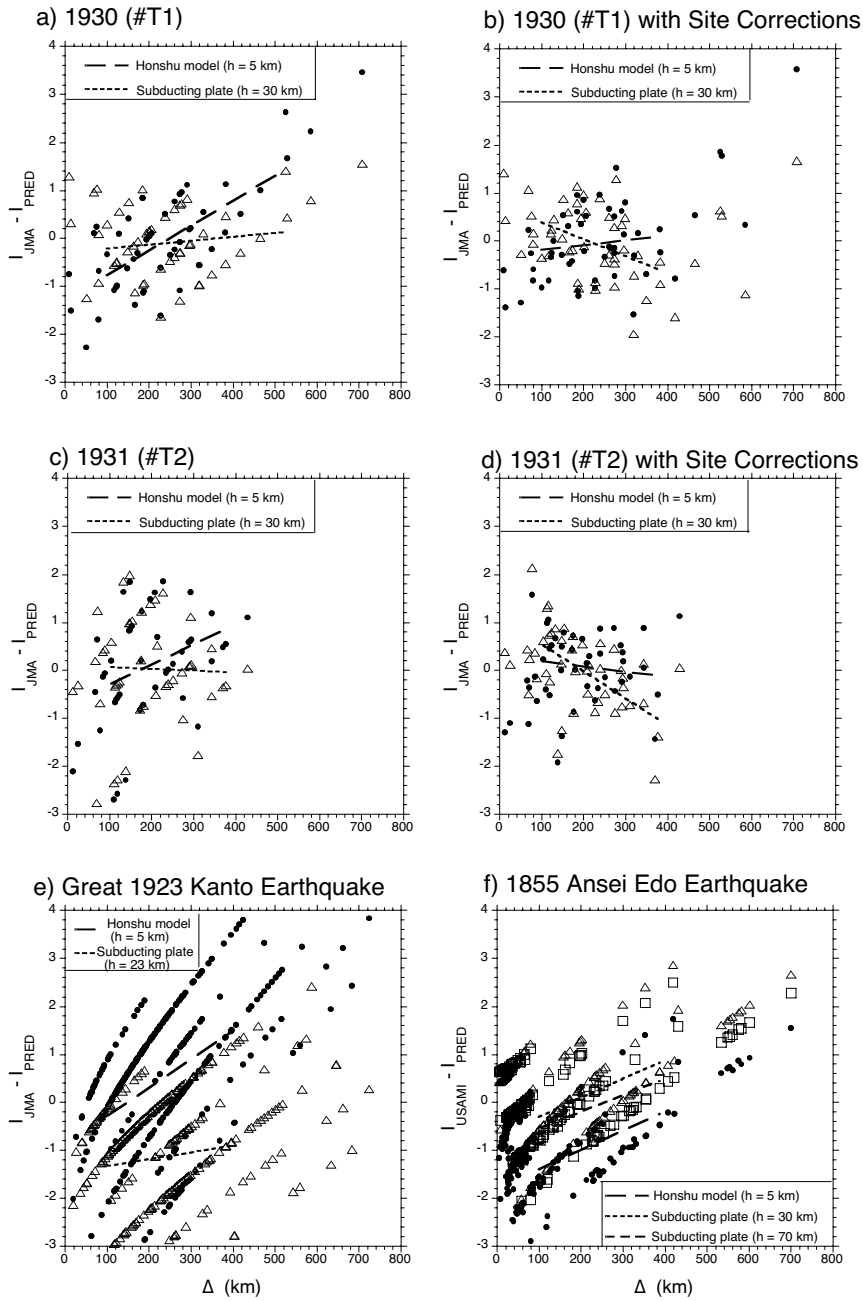


Figure 22